

**DUPLICATE COPY**

(2)

AD-A233 153

## THE STRUCTURE OF ATMOSPHERIC DIFFUSION AT REGIONAL SCALES

## FINAL TECHNICAL REPORT

F. A. GIFFORD

31 JANUARY 1991

U. S. ARMY RESEARCH OFFICE

CONTRACT NO. P-27096-GS-S

APPROVED FOR PUBLIC RELEASE;

DISTRIBUTION UNLIMITED

**DTIC**  
**S** **ELECTE** **D**  
MAR 18 1991  
**D**

## REPORT DOCUMENTATION PAGE

1a. REPORT SECURITY CLASSIFICATION Unclassified		1b. RESTRICTIVE MARKINGS	
2a. SECURITY CLASSIFICATION AUTHORITY		3. DISTRIBUTION/AVAILABILITY OF REPORT Approved for public release; distribution unlimited.	
2b. DECLASSIFICATION/DOWNGRADING SCHEDULE			
4. PERFORMING ORGANIZATION REPORT NUMBER(S)		5. MONITORING ORGANIZATION REPORT NUMBER(S) ARO 27096.1-G5-S	
6a. NAME OF PERFORMING ORGANIZATION Franklin A. Gifford	6b. OFFICE SYMBOL (if applicable) NA	7a. NAME OF MONITORING ORGANIZATION U. S. Army Research Office	
6c. ADDRESS (City, State, and ZIP Code) 109 Gorgas Lane Oak Ridge, TN 37830		7b. ADDRESS (City, State, and ZIP Code) P. O. Box 12211 Research Triangle Park, NC 27709-2211	
8a. NAME OF FUNDING/SPONSORING ORGANIZATION U. S. Army Research Office	8b. OFFICE SYMBOL (if applicable)	9. PROCUREMENT INSTRUMENT IDENTIFICATION NUMBER DAAL03-90-C-0018	
8c. ADDRESS (City, State, and ZIP Code) P. O. Box 12211 Research Triangle Park, NC 27709-2211		10. SOURCE OF FUNDING NUMBERS PROGRAM ELEMENT NO. PROJECT NO. TASK NO. WORK UNIT ACCESSION NO.	
11. TITLE (Include Security Classification) The Structure of Atmospheric Diffusion at Regional Scales			
12. PERSONAL AUTHOR(S) F. A. Gifford			
13a. TYPE OF REPORT Final Technical	13b. TIME COVERED FROM 90 Jul 01 TO 90 Dec 31	14. DATE OF REPORT (Year, Month, Day) 1991, January 31	15. PAGE COUNT 39
16. SUPPLEMENTARY NOTATION The view, opinions and/or findings contained in this report are those of the author(s) and should not be construed as an official Department of the Army position, policy, or decision, unless so designated by other documentation.			
17. COSATI CODES FIELD GROUP SUB-GROUP		18. SUBJECT TERMS (Continue on reverse if necessary and identify by block number) Regional-scale atmospheric turbulence; plume diffusion; fractional Brownian motion; diffusion modeling; fractal dimension	
19. ABSTRACT (Continue on reverse if necessary and identify by block number) The NOAA/ACURATE data, nineteen-month long series of 12-hour averaged Kr-85 air-concentration measurements at five sites up to 1050 km downwind of a source near AIKEN SC, are analyzed by a technique of fractal geometry, the renormalized-range statistic R/S. Fractional Brownian motion (Hurst) exponents H equal to about 0.35 are found for atmospheric eddy sizes of several hundred km, the enstrophy-cascade range, and these increased to H-values of about 0.45 for larger-scale motions. Corresponding fractal dimensions, D, equal about 1.65 and 1.55. Related power spectra and auto-correlations are discussed. The fractal indices can be applied in numerical diffusion models using available computer algorithms. Examples of R/S-analysis of short-range, rapid-response atmospheric diffusion observations are compared with the ACURATE results.			
20. DISTRIBUTION/AVAILABILITY OF ABSTRACT <input type="checkbox"/> UNCLASSIFIED/UNLIMITED <input type="checkbox"/> SAME AS RPT. <input type="checkbox"/> OTIC USERS		21. ABSTRACT SECURITY CLASSIFICATION Unclassified	
22a. NAME OF RESPONSIBLE INDIVIDUAL		22b. TELEPHONE (Include Area Code)	22c. OFFICE SYMBOL

UNCLASSIFIED

SECURITY CLASSIFICATION OF THIS PAGE

UNCLASSIFIED

SECURITY CLASSIFICATION OF THIS PAGE

Accession For	
NTIS CRA&I	<input checked="" type="checkbox"/>
DTIC TAB	<input type="checkbox"/>
Unannounced	<input type="checkbox"/>
Justification	
By	
Distribution	
Availability Codes	
Dist	Avail and/or Special
A-1	

CONTENTS



PAGE NO.

1. INTRODUCTION.....	5
2. THE NOAA/ACURATE DATA.....	6
3. FRACTAL DIMENSION OF ATMOSPHERIC CLOUDS.....	8
4. BROWNIAN MOTION IN ATMOSPHERIC DIFFUSION MODELING.....	10
5. SPECTRA AND CORRELATIONS.....	12
6. RENORMALIZED RANGE (R/S) ANALYSIS.....	13
7. R/S ANALYSIS OF SOME SMALL-SCALE, HIGH FREQUENCY DATA...	15
8. SUMMARY AND CONCLUSIONS.....	16
9. ACKNOWLEDGEMENTS.....	17
10. BIBLIOGRAPHY.....	17

## FIGURE LEGENDS

Figures 1 to 5: Twelve-hour averaged  $Kr^{85}$  concentrations at Fayetteville NC (FAY), Tarboro NC (TAR), Norfolk VA (NOR), Salisbury MD (SAL), and Murray Hill NJ (MUR), respectively. Concentration units are  $0.1 \text{ picocurie/m}^3$ . Time is given in halfdays (12-hour periods) starting from the first record chosen (cf. Table I).

Figure 6: Twelve-hour averaged  $Kr^{85}$  source strengths, curies/hour, at the Savannah River Plant (SRP) for the ACURATE data period.

Figure 7: Fractal Brownian motion time series for various H-values, from Barnsley, et al. (1988).

Figures 8 to 12: Power spectra of the ACURATE concentration data of Figures 1 to 5. Spectral density, in units of  $\text{concentration}^2$  per frequency unit, is plotted against frequency, per halfday.

Figure 13: Power spectrum of the SRP source strength data of Fig. 6,

in units of concentration<sup>2</sup> per frequency unit.

Figure 14: Autocorrelation curves for the ACURATE stations, including the SRP source.

Figures 15-19: Renormalized-range,  $R/S$ , as defined by Eq. 4, for the ACURATE stations.

Figure 20: Renormalized-range,  $R/S$ , as defined by Eq. 4, for the SRP source strengths.

Figure 21: Time series of  $SF_6$  concentrations measured 100 m downwind from a steady, ground-level, point source.

Figure 22: Renormalized-range,  $R/S$  statistic for the concentration data of Fig. 21.

Figure 23: Two-minute series of water-vapor flux values measured near the ground over an irrigated field.

Figure 24: Renormalized-range,  $R/S$  statistic for the water-vapor flux data of Fig. 23.

## TABLES

TABLE 1: SAMPLING POINTS OF THE ACURATE DATA..... 7

TABLE 2: VALUES OF THE HURST EXPONENT,  $H$ , SPECTRAL SLOPE,  $B$ , AND FRACTAL DIMENSION,  $D$ , FOR TIME SERIES..... 11

## 1. INTRODUCTION

Atmospheric turbulence and diffusion differ from their wind-tunnel counterparts in significant ways, caused primarily by the strong stabilizing influence of the earth's rotation on the larger-scale eddy motions. In addition, theoretically idealized flows such as stationary, homogeneous turbulence, or unbounded shear flows, which can be simulated quite satisfactorily in a wind-tunnel, are found to occur in the atmosphere very infrequently, and then only over very small fractions of the total turbulent volume. Thus, turbulent flows that are well understood from a theoretical or an experimental point of view are of only limited applicability to atmospheric turbulence and diffusion problems.

In very general terms, turbulent tropospheric motions appear to be of two kinds: large, quasi-horizontal, essentially two-dimensional, random eddy motions with length scales greater than several hundred kilometers; and smaller, three-dimensional random motions. The former cascade eddy enstrophy (mean-squared random vorticity) from the very large scale of eddy kinetic-energy generation (several thousand km) to scales of a few hundred km. The latter "dissipate" this random vorticity by rapidly attenuating, distorting, and concentrating it and-cascading the eddy-kinetic energy to the very small ( $< 1$  cm) scale of viscous dissipation. Natural or man-made clouds diffusing in this atmospheric field of random eddies in effect sample the turbulence structure through an ever-increasing volume of the atmosphere. At first, as the cloud spreads in the energy-cascade region, cloud growth by relative diffusion is rapid because the range of eddy sizes present always includes those that are just the size of the plume (Batchelor, 1952). Later, the cloud expands into the range of the enstrophy-cascading eddies. This range is characterized by rapid distortion, due to the large eddies, accompanied by diffusion at a reduced rate; large clouds quickly develop very irregular outlines, as is clear from the distorted shapes of the volcano plumes studied by Gifford (1989) and of the Chernobyl cloud (Smith, 1989). The usual cloud diffusion models, which have been developed in effect for the small-scale end of the energy-cascade range of eddies, do not describe the evolution of clouds spreading into the enstrophy-cascade region.

NOAA scientists conducted a series of diffusion experiments of increasingly large scale to study this problem; the ACURATE, CAPTEX, and ANATEX projects. The ACURATE (for Atlantic Coast Unique Regional Atmospheric Tracer Experiment) results include 19-month series of 12-hour averaged  $\text{Kr}^{85}$  concentrations measured at ground level at five observation points downwind of the Savannah River Plant at Aiken, SC. Observation sites ranged from Fayetteville, NC to Murray Hill, NJ, about 1100 km downwind. This report presents an analysis of these concentration time-series using a technique suggested by the recently-developed theory of random fractals, the so-called

"renormalized-range" statistic.

## 2. THE NOAA/ACURATE DATA

To clarify the complicated behaviour of the spreading of large clouds in the troposphere, as well as to support the diffusion modeling required by a host of important environmental problems of ever-increasing scale, it has become necessary to study tropospheric turbulence and diffusion to longer and longer distances from pollutant sources. This need was underscored by the recent air pollution disasters at Chernobyl and Bhopal. The NOAA experiments were designed primarily to produce diffusion-model validation data, and several comparisons have been published. But the data, especially the ACURATE results, are also a valuable archive of basic information on the detailed structure of atmospheric turbulence and diffusion (Heffter, et al., 1984).

In general, measuring diffusing clouds at large distances from a source requires somewhat heroic experimental arrangements, such as deploying hundreds of ground samplers or using several aircraft. Consequently the few completed experimental programs, summarized for instance by Gifford (1985), have produced very limited examples - partial measurements of only a few clouds for limited periods of time. In contrast the ACURATE program, using a  $Kr^{85}$  source-of-opportunity, measured downwind plume concentrations at five stations for over a year and a half. Moreover precise and detailed source-output data are available.  $Kr^{85}$  is in many ways an ideal atmospheric tracer, being long-lived, gaseous, non-reactive, and measurable at very low concentrations. Even though the source strength varied considerably, the time series of measured, 12-hour averaged  $Kr^{85}$  values must contain large amounts of information on plume structure, and consequently the structure of turbulence, particularly in the enstrophy-cascade region.

The ACURATE data, as reported by Heffter, et al. (1984), consist of measurements of  $Kr^{85}$  emitted from the Savannah River Plant (SRP), a production facility of the U. S. Department of Energy located some 35 km SE of Aiken, SC. Concentrations were averaged over 12-hour periods beginning at 0200Z and 1400Z, between March 1, 1982 and September 30, 1983 except at Murray Hill, where 24-hour averaged samples were taken and recorded as equal 12-hour values. The sampling points extended downwind from the source at the Savannah River Plant in an approximately north-easterly direction, at the distances and locations given in Table I. Of the 5 times 1158 possible concentration samples, 3858 non-zero values were archived. All these plus the source strength data are tabulated in the report, which provides much additional background of the experiment.

TABLE I  
SAMPLING POINTS OF THE ACURATE DATA

Station	(Abbrev.)	Distance, km	Length of record, 12-hour periods
Savannah River Plant	(SRP)	0	1158
Fayetteville, NC	(FAY)	325	240 (18) *
Tarboro, NC	(TAR)	475	311 (555)
Norfolk, VA	(NOR)	635	512 (578)
Salisbury, MD	(SAL)	790	408 (685)
Murray Hill, NJ	(MUR)	1050	944 (22)

\* (Record number of first concentration in each series)

The  $Kr^{85}$  data for the five ACURATE stations were prepared in the following way, to make them suitable for the proposed analysis. Leading and trailing zeros of each series were first removed. Then the data were inspected to identify periods containing at most a few single- or double-zero entries. Since  $Kr^{85}$  has a measurable background, zeros at the sampling points were used to indicate missing data. The longest period of record so defined for each station was chosen for analysis. For MUR this is nearly the entire period of record, a series of 944 12-hour averages. Other stations' records yielded various shorter periods, as indicated in Table I above. Numbers in parentheses in the Table indicate the record number of the first non-zero, 12-hour averaged concentration value that was used at each site. The single and double zeros in all these records were then filled in by linear interpolation between adjoining, non-zero values. Figs. 1-5 display the resulting time series of 12-hour averaged concentration values. In general the  $Kr^{85}$  concentration values all follow a pattern of irregular variation around a value on the order of 18 or 19 picocuries/meter<sup>3</sup> when the plume is not present, and increase sharply to peaks up to several times that when it is. The global background of  $Kr^{85}$  varies with latitude and location. Heffter, *et al.* (1984) assign the value 19 picocuries/meter<sup>3</sup> as the "background upper limit" of the ACURATE observations. The presence of the plume generally results in elevated concentration values over at least three successive (12-hour) data periods, and so occasional interpolation over one or two missing data values seems to be acceptable. The 12-hour averaged source-strength data, Figure 6, have been plotted without alteration, since zeros of these data ordinarily indicate zero emissions.

Figures 1 through 5 have some qualitative properties worth noticing. There is a discernible increase in the time between concentration peaks with increasing distance, which agrees very well with the intuitive idea that plume spreading and meandering are caused by the larger and larger eddies encountered downwind. The frequencies of concentration maxima, defined arbitrarily as values above 21 pc/m<sup>3</sup>, at each sampling location are 0.14, 0.10, 0.06, 0.05 and 0.02 per day at FAY, TAR, SAL, NOR and MUR respectively, a roughly linear decrease with distance. The relation of these large-scale plume fluctuations to those measured at much smaller scales, in the 50-100 m range by Hanna and Insley

(1989), up to a kilometer by Mylne (1990), and from 10 to 70 km by Mueller and Reisinger (1986), is an interesting subject for future study. Small-scale concentration variability is present at all the stations and seems to decrease in amplitude slightly with distance. This variability is however much less than that of the short-term variation of the source strength, as can be seen in Figure 6.

The ACURATE concentration data, because they are 12-hour averages, can be expected to yield structural information on atmospheric motions and diffusion at correspondingly large size scales. Concentration is a scalar property of the turbulence. The method of realizing this structural information depends on some recent developments in the theory of random fractals, cf. Mandelbrot(1982), Feder(1988), Barnsley, et al.(1988), in which it is shown that the fractal dimension of a passive scalar function of the turbulence such as these concentration measurements is directly related to that of the turbulence itself. Consequently analyses of the concentration-time series provide equivalent measures of the turbulence structure; in the case of the ACURATE data this is estimated to correspond to eddy scales ranging upward from about 200 km, assuming a typical transport wind of about 18 km/hr.

### 3. FRACTAL DIMENSION OF ATMOSPHERIC CLOUDS

The observed shapes of energy spectra in the earth's troposphere, especially the extensive GASP spectra (Nastrom and Gage, 1986), strongly suggest a large-scale, enstrophy-cascade range and a smaller-scale, energy-cascade range of turbulent atmospheric winds extending in broad spectral regions above and below a fairly wide transition region at a scale of about 300-500 km. The largest atmospheric eddies, at scales just below the scale at which kinetic energy is generated in the atmosphere, are essentially two-dimensional in structure because of their great size, several thousand km. They are believed to create a flux of random vorticity, or eddy enstrophy, toward smaller scales of motion. Such motions have been called geostrophic turbulence (Charney, 1971). At scales of several-hundred kilometers, eddies begin to appear that are small enough to be affected by the essentially 3-dimensional process of vortex stretching and deformation by the strain-rate field of the larger eddies. This process increasingly concentrates and deforms the eddy-vortex structure and results in an energy cascade toward the minute, dissipation scale of eddy motions. Enstrophy and energy transfer in these two broad spectral regions can be described solely in terms of the "similarity" parameter appropriate to each range, the averaged eddy-enstrophy transfer and eddy-energy transfer rates (Gifford, 1988). The length scale separating these two cascade ranges corresponds closely to the time scale of the earth's rotation, the reciprocal of the Coriolis parameter,  $1/f$ , which has been shown (Gifford, 1984) to equal the outer, or integral scale of atmospheric diffusion.

This suggests that long series of concentration values measured at fixed points, such as the ACURATE data, which also depend on the

structure and dynamics of turbulence in the cascade ranges, will reflect a self-similar (more precisely a self-affine) structure, as has been discussed by Barnsley, et al. (1988) and Feder (1988). These concentration-time series record, in effect, a one dimensional measure of the spatial structure of the evolving  $Kr^{85}$  cloud. Because the measurement in time bears an unknown scale relationship to the corresponding spatial measurement, it is not strictly correct to speak of (spatial) self-similarity, and so the closely-related concept of self-affinity has been invoked (Mandelbrot, 1982). For a concentration-time series to be self-affine, it must have the property that changes in concentration depend on time in such a way that in a statistical sense, for any two times  $t_1$  and  $t_2$ ,

$$C(t_2) - C(t_1) \propto (t_2 - t_1)^H, \quad (1)$$

The similarity constant  $H$ , the so-called Hurst exponent, is related to fractal dimension,  $D$ , by

$$D = 2 - H. \quad (2)$$

the idea of fractal dimension was introduced by Mandelbrot (1982) to account for the fact that natural shapes, including the outlines of clouds, the shapes of snowflakes and radar rain echos, and many other atmospheric phenomena, can not be measured by the Euclidean metric that applies to smooth, geometrical objects. The fractal dimension, which exceeds the Euclidean dimension (and is usually fractional), is in effect a measure of an object's irregularity. Lovejoy (1982) showed, by comparing the areas and perimeters of radar and satellite images of precipitation and cloud patterns, that the fractal dimension,  $D$ , of the perimeters of clouds and rainbands and, by inference, of the atmospheric turbulent eddies that drive those features, equals 1.35 over a broad range of eddy scales. Gifford (1989) showed that this result applies closely up to linear scales of about 300-400 km, or time scales a few times  $10^4$  seconds, but that at larger scales, in the enstrophy-cascade region, Lovejoy's data support  $D \approx 1.8$ , indicating turbulence of a markedly different type at these larger scales. Since these examples of fractals refer to cloud perimeters, whose Euclidean dimension is one, they lie between one and two. The corresponding result for the areas of cloud cross-sections would be 2.35 and 2.78; and for cloud volumes there will naturally be another unit increase to these dimensions. Ludwig (1989) has provided an excellent review of the considerable and rapidly expanding literature on atmospheric fractals and their properties, and a general review of applications to geology and geophysics was given by Turcotte (1989).

Squaring equation (1) and averaging gives

$$\langle \delta C^2 \rangle \propto \delta t^{2H}, \quad (3)$$

since  $H$  is defined to be a constant of this idealized process;  $\delta C$  is the concentration increment over the time lag,  $\delta t = t_2 - t_1$ ; and  $\langle \dots \rangle$  indicates averaging over all possible values. Also from

Eq.(1), the so-called "renormalized-range" statistic (Mandelbrot, 1982) can be written as

$$[C_{\max}(\tau) - C_{\min}(\tau)]/\sigma_C(\tau) = R(\tau)/S(\tau) = b\tau^H \quad (4)$$

where  $R$  is the range,  $S$  ( $=\sigma_C$ ) is the standard deviation of  $C$  during the time interval  $\tau=t_1-t_0$ , and the interval  $\tau$  is always measured from the initial value of the series. Logarithmic plots of  $R/S$  vs.  $\tau$ , or of  $\langle \delta C^2 \rangle^{1/2}$  vs.  $\delta t$ , should contain broad linear ranges if, in these ranges, atmospheric turbulent motions are self-similar. Atmospheric values of the similarity exponent  $H$ , and of the fractal dimension  $D$  of atmospheric turbulence, follow directly from these slopes, since in general  $D = E+1-H$ , where  $E$  is the Euclidean dimension of an object (Mandelbrot, 1982).

#### 4. BROWNIAN MOTION IN ATMOSPHERIC DIFFUSION MODELING

All atmospheric diffusion modeling makes use of the assumption of Brownian motion. This is done either directly, as in models of the Lagrangian particle motion (e.g. Hanna, 1979; Gifford, 1982), or indirectly, through the assumption of Gaussian turbulence statistics in plume models or by use of K-theory. The turbulent motion  $v(t)$ , and consequently the position of a pollutant particle, can be expressed as

$$v(t+\delta t) = v(t) + r(t) \quad (5)$$

(Hanna, 1979), where  $r(t)$  is a random velocity with Gaussian statistics;  $r(t)$  is the integral of a random acceleration,  $a(t)$ , having Brownian motion, or "white noise" statistics, i.e.

$$r(t) = \int_{-\infty}^t a(x) dx \quad (6)$$

Integration of  $v(t)$  in turn gives the value of the displacement,  $y(t)$ , of a particle from the axis of the mean wind, since  $dy(t)/dt = v(t)$ . Such a Gaussian random process has the well-known properties:

$$\langle y(t) - y(t_0) \rangle = 0$$

and

$$\sigma_y^2 = \langle (y(t) - y(t_0))^2 \rangle \propto t \quad (7)$$

Mandelbrot (1982) proposed the following generalization of the Brownian motion model;

$$\langle [y(t) - y(t_0)]^2 \rangle \propto t^{2H} \quad (8)$$

where  $0 < H < 1$ . From Eq.(7),  $H$  is equal to  $1/2$  for ordinary Brownian motion. In nature  $H$  does not usually equal  $1/2$ ; natural noise signals are ordinarily not white. By fitting various kinds of long, natural time-series (river discharges, tree-ring data, varves, etc.) to Eq.(4), it has been found (Feder, 1988) that often  $H \approx 0.7-0.8$ . The assumption that atmospheric turbulence is of the Brownian motion type, implying that  $H = 1/2$ , is known to result in fairly good estimates of atmospheric diffusion (e.g. Barr and Gifford, 1987; Gifford, 1985), which is why it is a staple of atmospheric modeling. Yet systematic departures are known to occur and must be considered by modelers. Theoretical arguments (Mandelbrot, 1983; Hentschel and Procaccia, 1983) in terms of fractal geometry for the special case of fully-developed homogeneous turbulence, not often realized in the atmosphere, indicate that  $H$  is on the order of  $1/3$ .

Figure 7, from Barnsley et al. (1988), illustrates fractional Brownian-motion (fBm) curves for a range of values of  $H$ . For  $H = 0.8$ , corresponding most closely to the river-discharge, varve, and tree-ring data, high-frequency spikes are small and the fBm curve is relatively smooth. For  $H = 1/2$ , the case of ordinary Brownian motion, all frequencies are equally represented. For  $H = 0.2$ , presumably closest to atmospheric turbulence, the fBm curve is decidedly rougher at all scales. Numerical algorithms for generating such fBm curves, developed at first for computer simulation of natural landscapes, can be found in Barnsley et al. (1988) and Feder (1988). Given suitable values of  $H$ , these algorithms can be introduced directly into Lagrangian diffusion models. There they will simply replace existing random-number generators such as the acceleration,  $a$ , in Eq. (6) to provide more realistic atmospheric turbulence simulation than the default assumption  $H = 1/2$ .

The physical meaning of  $H$  is perhaps most easily conveyed by relating fBm to the more familiar power- or energy-spectrum representation. In a similarity region of the spectrum the energy-density has a power-law relationship to frequency, proportional to  $1/f^\beta$ , where  $f$  is frequency and  $\beta$  is a constant similarity exponent. The fractal dimension of the energy spectrum in such a region can be shown (Mandelbrot, 1982) to be given by

$$D = E + 1 - H = E + (3-\beta)/2 \quad (9)$$

where  $E$  is the spectrum's Euclidean dimension. For time spectra,  $E = 1$  and  $D = 2-H$ . Since  $0 < H < 1$ , the array of values shown in Table II can be developed.

TABLE II

VALUES OF THE HURST EXPONENT,  $H$ , SPECTRAL SLOPE,  $\beta$ , AND FRACTAL DIMENSION,  $D$ , FOR TIME SERIES

Power Law Parameter	Extreme Value	Kolmogoroff Turbulence	Brownian Motion	Extreme Value
$H$	1	$1/3$	$1/2$	1
$\beta$	1	$5/3$	2	3
$D$	2	$5/3$	$3/2$	1

$H = 1/3$  is the theoretical value for Kolmogoroff turbulence, i.e. locally-homogeneous flow with an inertial-range spectrum.  $H = 1/2$  corresponds, as pointed out above, to the spectrum of ordinary Brownian motion.

The autocorrelation curve is also governed by  $H$ . For  $H = 1/2$  the fBm is uncorrelated; future values are completely independent of the past. For  $H > 1/2$  the fBm exhibits persistence, so that departures from the mean tend to be followed by even larger departures. In the limit of large time, the correlation remains positive. For  $H < 1/2$  the limiting value of the correlation is negative, indicating antipersistence; large departures tend to be followed by a return toward the central value.

Until the development of fractal geometry there has been no quantitative, explicit way to take such differences in the shape of turbulence functions into account in models and indeed little by way of quantitative perception of their existence in atmospheric flows. By applying the theoretical results sketched briefly above to the ACURATE data, we can hope to find out how  $H$  and  $D$  behave at large scales in the troposphere, so that this information can be incorporated into atmospheric diffusion models. The following results indicate something of what can be accomplished using the fractal methodology.

## 5. SPECTRA AND CORRELATIONS

Figures 8 through 13 are power spectra of the ACURATE concentration and source-strength time series, made using the Cooley-Tukey FFT algorithm developed by Yamartino (1988). Means have been removed, and the spectral densities smoothed, using the standard procedures recommended in this reference. Spectra for stations NOR and SAL have been smoothed twice to make them a little more intelligible. The spectra have been plotted in logarithmic coordinates in the hope of finding linear, and therefore similarity regions at their high frequency ends, corresponding to the enstrophy-cascade region. Of the five spectra, only those for TAR and MUR show reasonably linear regimes at high frequencies, Figs. 8 and 9. The slopes in

each instance are very close to the value  $\beta = 3.0$  in frequency ranges from about daily to once per 2.5 days.

Autocorrelations of the same data are shown in Figure 14. The autocorrelation of the source emissions at SRP is included for comparison. The concentration correlations all have similar, exponential shapes; they each drop rapidly, although at substantially differing rates, and approach zero from very slightly negative values. The source autocorrelation also drops rapidly, as was to be expected from the appearance of Fig. 6, the emissions-time plot. Its behavior thereafter is however quite different from that of the concentration correlograms, giving some hope that the latter have been formed primarily by atmospheric effects. The emissions data, Fig. 6, suggest that source emissions have a white-noise character but with substantial nonstationarity, no doubt associated with the evident long-term changes in emissions patterns.

Rationalizing the shapes of these conventional descriptors of stochastic behavior is not the principal business of this study and will not be pursued further here, except to remark that the unsteadiness of the SRP sources is a problem, the more so the shorter the distance downwind. Meaningful interpretations in terms of spectral slope, or the scales of the correlograms, will obviously be very difficult to come by. At a guess, it might be useful to identify more nearly stationary sub-periods for spectral analysis, based on the emissions patterns of Fig. 6. Judging by the interesting numerical experiments by Fox (1989), who compared spectral and fractally derived similarity exponents for computer-generated unstationary series, fractal methods may be less troubled by the problem of nonstationarity.

## 6. RENORMALIZED RANGE (R/S) ANALYSIS

The renormalized-range statistic  $R/S$ , defined by Eq. 4 above, is formed from a time series of observations of a quantity by determining a new series whose members, up to a given member of the original series,  $\tau$ , consist of the ratio of the range,  $R$ , i.e. the largest minus the smallest value, to the standard deviation,  $S$ , of the values of the series up to that same member. As a measure of dispersion, the range has chiefly been used in quality control applications involving short data runs. Its applicability to the fractal analysis of geophysical time series was pointed out by Mandelbrot (1982) and is discussed in the references already given, especially Feder (1988).

Figures 15-20 are renormalized-range plots of the ACURATE data, including (Fig.20) the emissions data. The  $R/S$  values are plotted on the same, logarithmic coordinates in each case, to facilitate comparisons among the various sites. The actual concentration-time series used are those illustrated in Figs. 1-6, which were also the basis for the spectral and autocorrelation analyses of the preceding section. A solid line connects all data points, and

segments chosen for power-law least-squares analysis are indicated by a dashed line of best fit. These segments are further delineated by having a selection of data points (in most cases every tenth point) plotted. The slopes of the best-fit lines, i.e. the values of the Hurst exponent,  $H$ , in Eq. 4, are tabulated in each figure.

The R/S curves for the ACURATE concentration data, Figs. 15-19, in spite of some irregularity in the sense of departures from strict power-law behavior, show a remarkably consistent pattern. Each is easily resolved by inspection into series of straight-line (i.e. power-law) segments connected by jumps, both upward and downward, to a new linear segment. The connecting segments last several days to a week or so and are irregular in shape, exhibiting no clear structural pattern. The linear segments, which indicate fractal (i.e. self-similar) behavior of the eddy motions at these scales, persist for periods that are usually on the order of several weeks but often last for months. The quality of the power-law curve fits in these linear segments is so high that it has not seemed worthwhile to bother calculating correlations, which obviously would equal unity to several significant figures. In a few instances the jump periods can be associated with aperiodic shifts in the emissions level (Fig. 6), but most jumps are related to the sudden onset of sharp concentration maxima, the spikes of Figs. 1-5. Considering the form of the R/S statistic, it is easy to understand how a concentration peak, caused by a swinging of the main  $\text{Kr}^{85}$  plume over a recording station, results in a sharp rise in R/S by increasing R more than S. Some of the downward jumps, which tend to be less abrupt and are often irregular, seem to be driven by the non-stationarity of the source term. Others could be the result of concentration spikes too small to increase the range but large enough to increase the standard deviation. The behavior of the source-strength R/S curve, Fig. 20, differs qualitatively from these concentration R/S patterns as indeed does the source-strength spectrum, Fig. 13, from the concentration spectra of Figs. 8-12.

Such comparisons of segments of R/S curves to equivalent parts of the original time series are possible because the R/S statistic preserves real-time relationships. This means that every point along the  $\tau$ -axis of an R/S graph corresponds to the same point of its original time axis. This property contrasts R/S sharply with the power-spectrum statistic, and makes it possible to associate particular features of R/S curves with specific values or ranges of the original time-series. As a result it can be seen that power-law, i.e. self-similar, behavior is characteristic of the concentration-time plots, and consequently of the eddy-structure at these large scales, most of the time. This interesting property can not be inferred from the energy spectra or autocorrelations.

The slopes of the linear segments in Figs. 15-19 show a weak tendency to increase slightly with the time interval,  $\tau$ , from  $H$ -values near 0.35 for R/S values calculated for intervals extending to two or three weeks to values near 0.45 or more for intervals extending to several months. The smaller values, by the reasoning outlined above, characterize atmospheric eddy motions at scales

corresponding to the enstrophy-cascade range. The larger values of  $H$  are associated with the largest scales of motions that influenced the  $Kr^{85}$  concentration data. Values of  $H = 0.3$  to  $0.4$  correspond to fractal dimensions  $D$  of  $1.6$  to  $1.7$ , in agreement with various other estimates, for instance Gifford (1989). One should, of course, interpret these results with caution. Fractal index values estimated from limited series of such highly variable data are not likely to be valid to much more than a single decimal place (cf. Mandelbrot, 1982), which means that the uncertainty of the  $H$ -values may be about  $\pm 0.1$ . Additionally, the ACURATE data are 12-hour averages, and neither sampling nor averaging properties of fractal statistics have been studied to any extent. Also it is desirable, according for instance to Feder (1988), to base estimates of  $R/S$  on much larger series of observations. The calculated  $R/S$  values are, moreover, limited by the fact that the interval  $\tau$  has been measured, in each instance, from the first value of the concentration-time series only, in order to preserve the time relationship pointed out above. Particularly for smaller values of  $\tau$ , other non-overlapping data periods could have been used and, in the interests of statistical reliability, this should be a future task. But even the limited evidence described here seems adequate to suggest the need to constrain stochastic elements of large-scale atmospheric diffusion models to agree with an  $H$ -value of  $0.3$  or  $0.4$  in the enstrophy-cascade range, rather than to depend solely on the default value of  $H = 1/2$ , for ordinary Brownian motion, that current diffusion-modeling practice in effect assumes.

## 7. R/S ANALYSES OF SOME SMALL-SCALE, HIGH FREQUENCY DIFFUSION DATA

There have, as far as the writer knows, been no previous studies of atmospheric tracer concentration data by the renormalized-range method, and so the somewhat complex shapes of the ACURATE-data  $R/S$  curves raise some interesting but difficult questions. Will similar patterns of power-law  $R/S$  behaviour interspersed with more-or-less rapid jumps in  $R/S$  level be found in the analysis of short-range, high-frequency concentration measurements? What  $H$ - and  $D$ -values will characterize time series of such data? Is the jump pattern peculiar to plume concentrations from isolated sources, or does it also occur for distributed sources of atmospheric emissions, such as area sources or line sources? Such questions underscore the desirability of applying the  $R/S$  analysis to a wide range of atmospheric turbulence and diffusion data. But to help put the present results into some kind of perspective, two further turbulence-data time series of atmospheric measurements have been analyzed.

Figure 21 is a time series of concentration measurements made under mid-day, convective conditions over desert terrain,  $175$  m downwind from a continuous point source near the ground. The concentrations were measured as part of a series of low-level  $SF_6$  tracer tests at Hanford, WA, using a continuous, very fast-response monitor. The resulting  $R/S$  values are shown in Figure 22, together with some typical, linear-segment slope values. We see that power-law, similarity behavior occurs; that it is interrupted by

jumps, as was true for the ACURATE data; and that, so far as can be concluded from a single run,  $H$  equals about 0.3 to 0.35 in this range of small-scale turbulent motions.

Figure 23 is a two-minute series of water-vapor flux values, measured by a very rapid response technique over an irrigated agricultural (cotton) field during early-morning conditions of developing convective instability. Corresponding  $R/S$  values, shown in Figure 24, after an initial few seconds of erratic behavior rise smoothly and linearly. In the range from 10 to about 120 seconds  $H$  is very close to 0.4, with no jumps during that period of measurement. Since the data are an example of area-source diffusion, the lack of jumps such as were found in the  $R/S$  analysis of the ACURATE data can be taken as at least a provisional indication that the jumps that are found in the ACURATE  $R/S$ -curves, and in Fig. 22 above, may be a feature of point-source diffusion. Further such  $R/S$  analyses of both point- and area-source diffusion should be made to explore this issue.

## 8. SUMMARY AND CONCLUSIONS

Nineteen-month series of 12-hour averaged  $Kr^{85}$  air concentration values, the NOAA/ACURATE data (Figs. 1-5), measured at five stations up to 1050 km downwind from the source at Savannah River, near Aiken SC (Fig. 6), have been analyzed by a method of fractal geometry, the renormalized-range statistic,  $R/S$  (Eq. 4). The resulting  $R/S$ -plots (Figs. 15-19) indicate that atmospheric diffusion at scales greater than several hundred km, in the enstrophy-transfer range of the troposphere's energy spectrum, is driven by large-scale, horizontal, self-similar eddies whose characteristic fractional Brownian motion exponent (Eq. 8) is in the range  $H = 0.3-0.4$ . This corresponds to a fractal dimension in the range  $D = 1.6-1.7$  for one-dimensional measures of the flow such as these concentration-time series. This is a useful result for large-scale atmospheric diffusion modeling, which currently assumes that ordinary Brownian motion (i. e.  $H = 1/2$ ) applies. Such Brownian motion is purely uncorrelated whereas actual atmospheric flows at these large scales exhibit antipersistence, i. e. a small negative correlation at large lagtimes, according to these results. The similarity exponent  $H$  seems to increase slightly with time scale, to values of 0.40-0.45 at the time periods in excess of a week or two, corresponding to the synoptic scales of eddy kinetic-energy generation.

The properties of atmospheric turbulent diffusion at scales between 100-200 km and 1000-2000 km have not been much studied. This range tends to fall into a gap between the statistical theories of planetary boundary layer turbulence and diffusion studies and the numerical-analytical solutions of large-scale modeling. PBL-scale diffusion models are pushed to, and in most cases probably beyond, the reasonable limits of their necessary assumptions at distances more than 20 or 30 km. And even the most venturesome

among synoptic-scale modelers perceive a fairly large-scale lower limit to their predictions of atmospheric motions, of perhaps 500 km at an optimistic estimate, because of inability of these models to resolve turbulence at smaller scales. But practical operational and regulatory problems are no respecters of such limitations and require diffusion estimates when and as needed. What is needed is a method for supplying the correct kind and degree of randomness to the diffusion models, according to the fractional Brownian motion properties of the atmosphere, at scales ranging upwards from a few tens of kilometers. This can be done by using fBm algorithms with appropriate H-values to simulate atmospheric turbulence statistics. Many more determinations of atmospheric values of H and D at various scales clearly need to be made. It is hoped that the above results can help both to characterize turbulent atmospheric motions at the troublesome intermediate scales in a way that can be put directly to work in diffusion models, and to encourage use of a potentially fruitful technique for analyzing atmospheric diffusion data of many kinds at all scales.

## 9. ACKNOWLEDGMENT

The writer is grateful to his colleagues of NOAA's Air Resources Laboratories, especially R. Draxler, J. Heffter, and L. Machta, for providing a file of the ACURATE data and sharing their first-hand knowledge of that project. B. Lamb, Washington State University, and D. Cooper, Los Alamos National Laboratory, very generously provided examples of short-range SF<sub>6</sub> concentrations and water-vapor flux measurements respectively, from current research projects. W. Bach, F. Ludwig, R. Draxler, and J. Heffter provided valuable critical comments and suggestions on a draft of this report. This study is supported by the U. S. Army Research Office.

The writer, F. A. Gifford, an independent, self-employed research worker, is the only participant in this project. The research involved no subcontracts, and no inventions or advanced degrees have resulted.

## 10. BIBLIOGRAPHY

Barnsley, M. F., R. L. Devaney, B. B. Mandelbrot, H.-O. Peitgen, D. Saupe, and R. F. Voss, 1988: The science of fractal images, Springer-Verlag, NY.

Barr, S. and F. A. Gifford, 1987: The random force theory applied to regional scale atmospheric diffusion, Atmos. Environ., U\21, 1737-1741.

Batchelor, G. K. 1952: Diffusion in a field of homogeneous turbulence, II. The relative motion of particles. Proc. Camb. Phil. Soc., U\48, 345.

Charney, J., 1971: Geostrophic Turbulence, J. Meteor., 1087-1095.

Feder, J., 1988: Fractals, 283pp, Plenum Press, NY.

Fox, C. G., 1989: Empirically derived relationships between fractal dimension and power law form frequency spectra, in Fractals in Geophysics, C. H. Scholz and B. B. Mandelbrot, Eds., pp 211-249, Birkhauser Verlag, Basel. [Reprinted from Pure and Applied Geophysics, 131, (1989).]

Gifford, F. A., 1982: Horizontal diffusion in the atmosphere: a Lagrangian, dynamical theory, Atmos. Environ., 16, 505-512.

Gifford, F. A., 1983: Atmospheric diffusion in the mesoscale range: the evidence of recent plume width observations, Preprint Vol., 6th Symp. on Turbulence and Diffusion, March 22-25, 1983, Amer. Meteor. Soc.

Gifford, F. A., 1984 The random-force theory: application to meso- and large-scale atmospheric diffusion, Boundary Layer Meteor., 30, 159-175.

Gifford, F. A., 1985: Atmospheric diffusion in the range 20 to 2000 km, in Air Poll. Modeling and its Applications, Plenum Press, pp. 247-265.

Gifford, F. A., 1988: A similarity theory of the tropospheric turbulence energy spectrum, J. Atmos. Sci., 45, 1370-1379.

Gifford, F. A., 1989: The shape of large tropospheric clouds, or "Very like a whale", Bull. Am. Meteor. Soc., 70, 468-475.

Hanna, S. R., 1979: Some statistics of Lagrangian and Eulerian wind fluctuations, J. Appl. Meteor., 18, 518-525.

Hanna, S. R. and E. M. Insley, 1989: Time series analysis of concentration and wind fluctuations. Boundary-Layer Meteorology, 47, 131-147.

Heffter, J. L., J. F. Schubert, and G. A. Mead, 1984: Atlantic Coast Unique Regional Atmospheric Tracer Experiment (ACURATE), NOAA Tech. Memo. ERL ARL-130, 60pp.

Hentschel, H. G. E. and I. Procaccia, 1983: Fractal nature of turbulence as manifested in turbulent diffusion, Phys. Rev. Letters, A, 27, 1266-1269.

Lovejoy, S., 1982: The area-perimeter relationship for rain and cloud area, Science, 216, 185-187.

Ludwig, F., 1989: Atmospheric fractals, a review, Environ. Software, 4, No.1 (March, 1989).

Mandelbrot, B. B., 1982: The fractal geometry of nature, 486 pp, W. H. Freeman Co., NY. [This is a revised edition of Fractals: Form, Chance and Dimension, 1977.]

Mueller, S. F. and L. M. Reisinger, 1986: Measured plume width versus sampling time: a look beyond 10 kilometers, Atmospheric Environment, 20, 895-900.

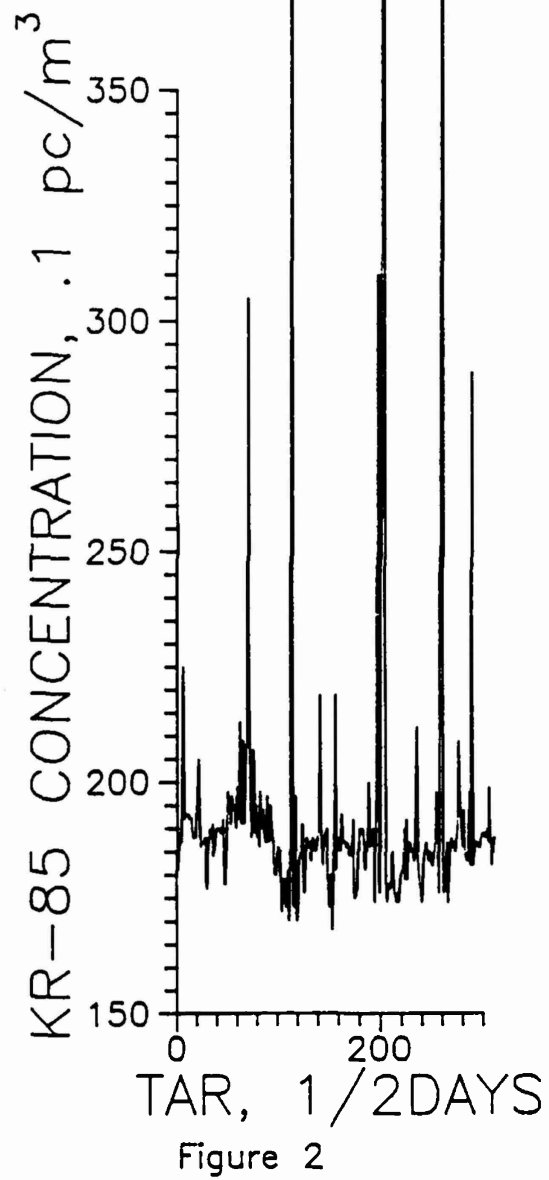
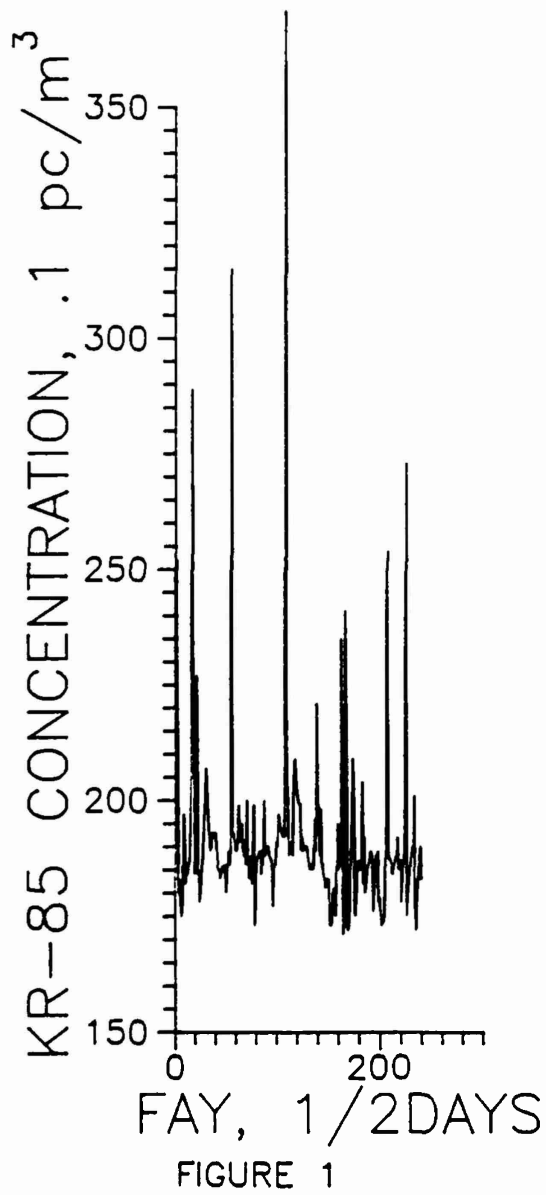
Mylne, K. R., 1990: Concentration fluctuation measurements of a tracer plume at up to 1 km range in the atmosphere, in Proc. of the Ninth Symposium on Turbulence and Diffusion, April, 1990, 168-171, American Meteor. Soc., 45 Beacon St., Boston, MA 02108.

Nastrom, G. D., and K. S. Gage, 1986: A climatology of atmospheric wavenumber spectra of wind and temperature by commercial aircraft, J. Atmos. Sci., 42, 950-960.

Smith, F. B., 1989: The deposition of Chernobyl cesium-137 in heavy rain and its persistent uptake by grazing sheep, Agricultural and Forest Meteorology, 47, 163-177.

Turcotte, D. L., 1989: Fractals in geology and geophysics, in Fractals in Geophysics, 171-196, Birkhauser Verlag, Basel [Reprinted from Pure and Applied Geophysics, vol. 131, 1989].

Yamartino, R., 1988: SIGMA-SPEC 2.2 Spectral Analysis Program, 8 pp., Sigma Research Corporation, 234 Littleton Road, Suite 2E, Westford, MA 01886.



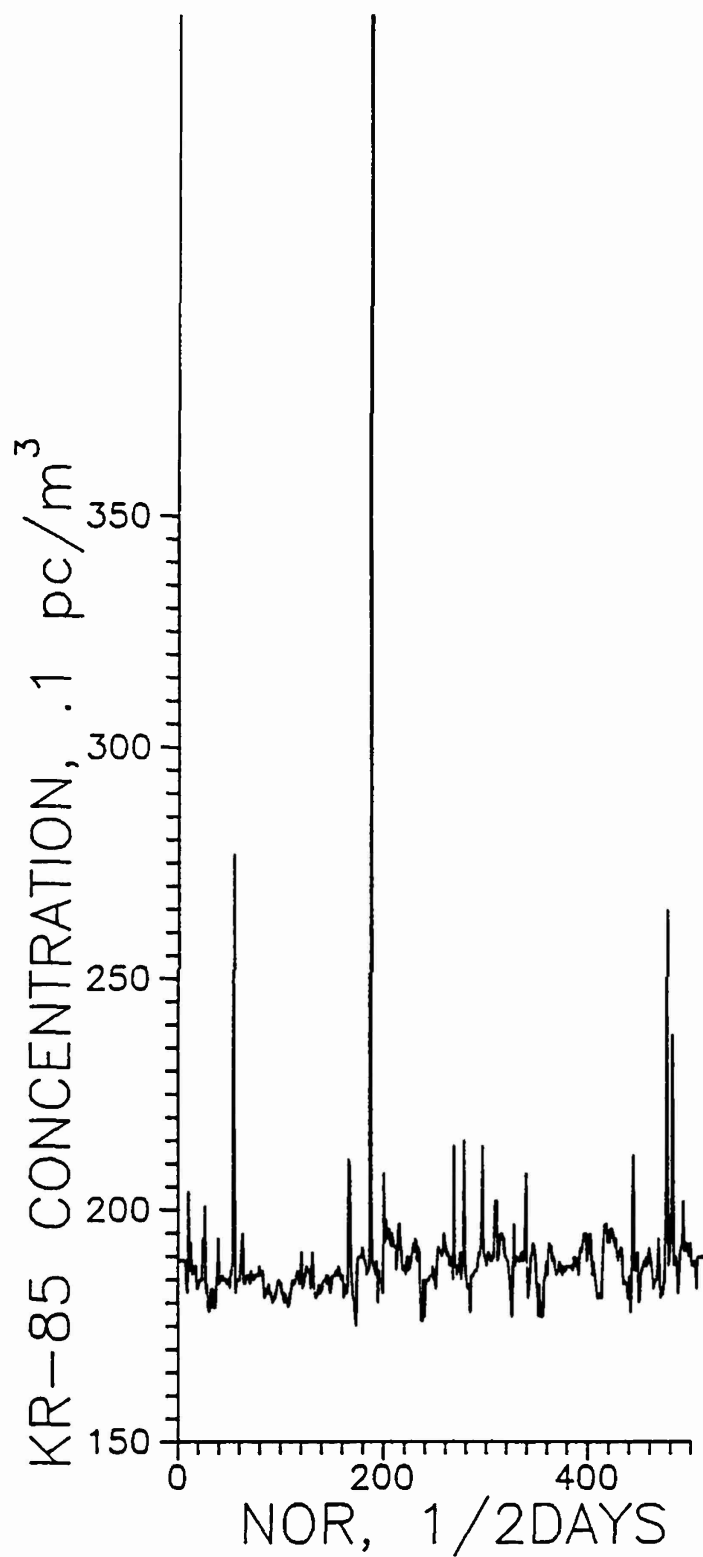


Figure 3

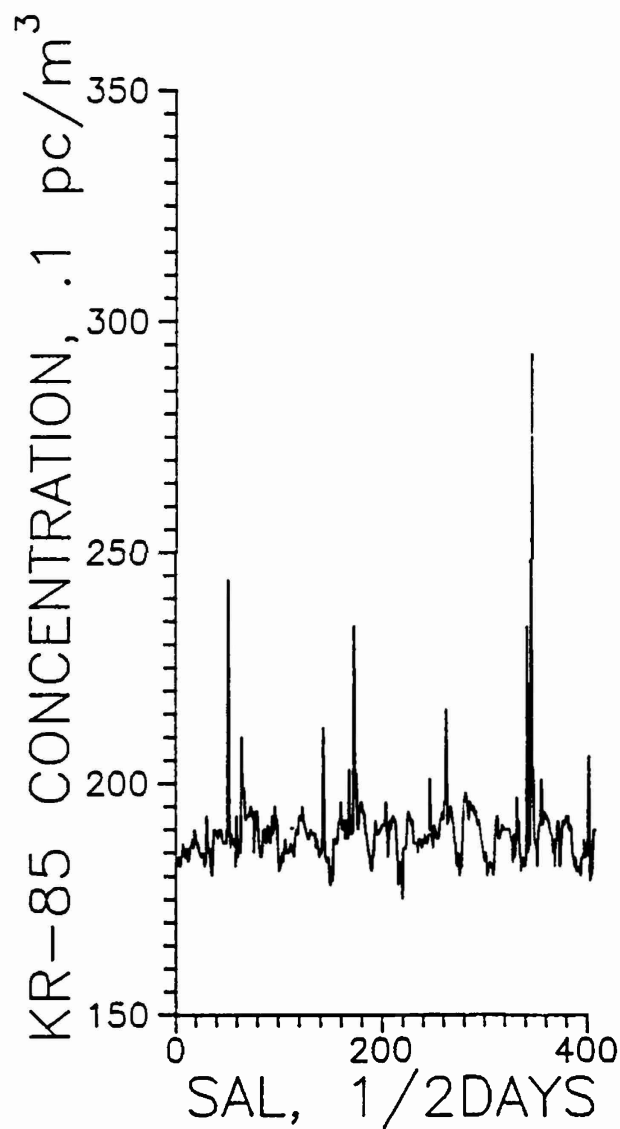


Figure 4

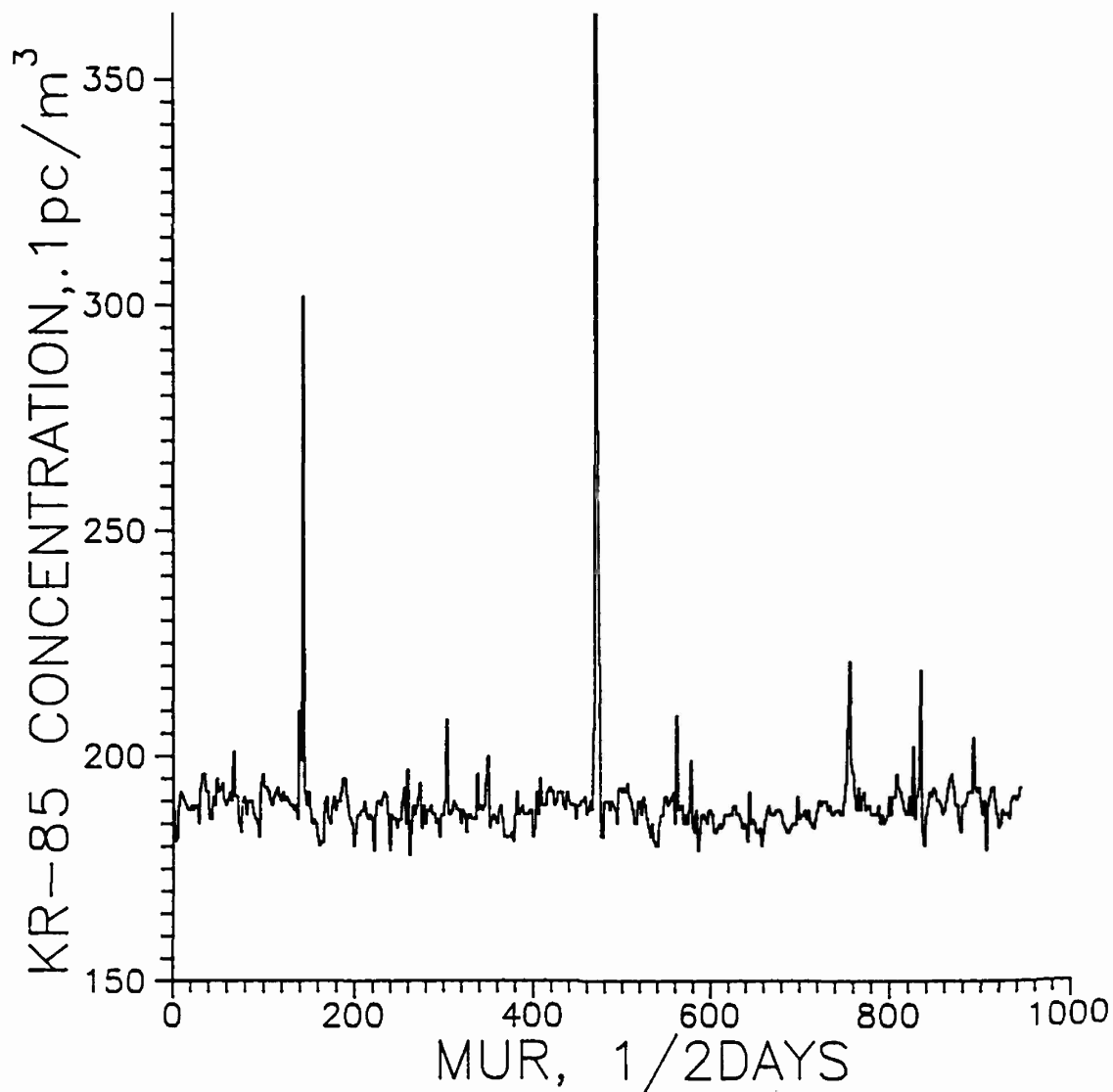


Figure 5

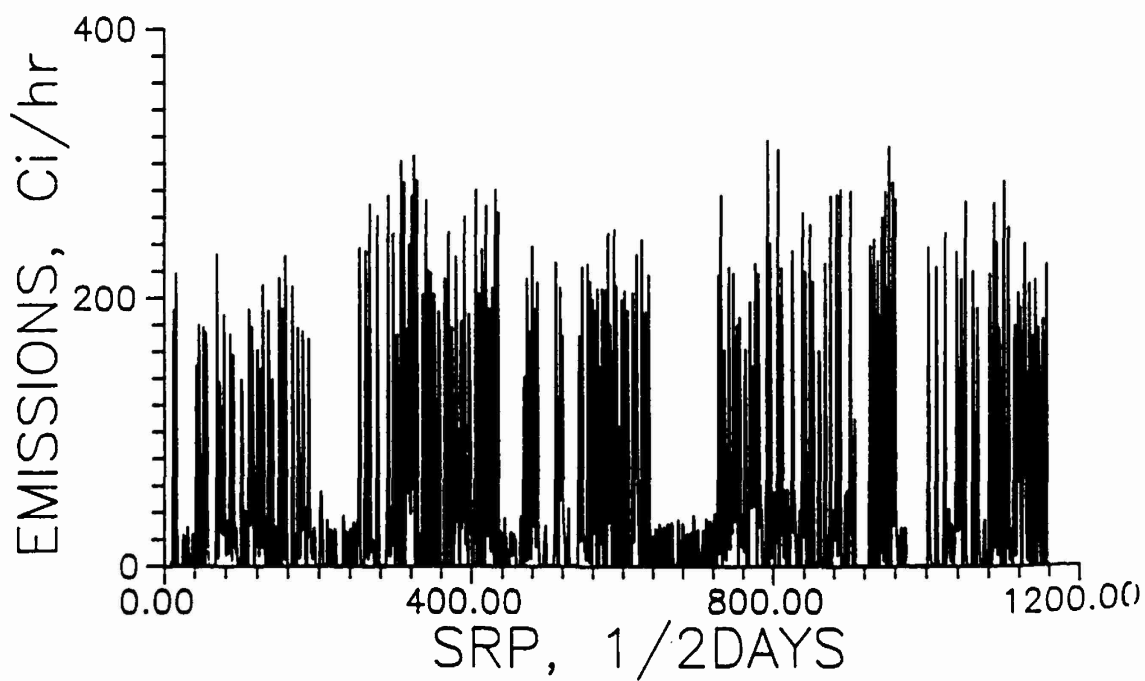
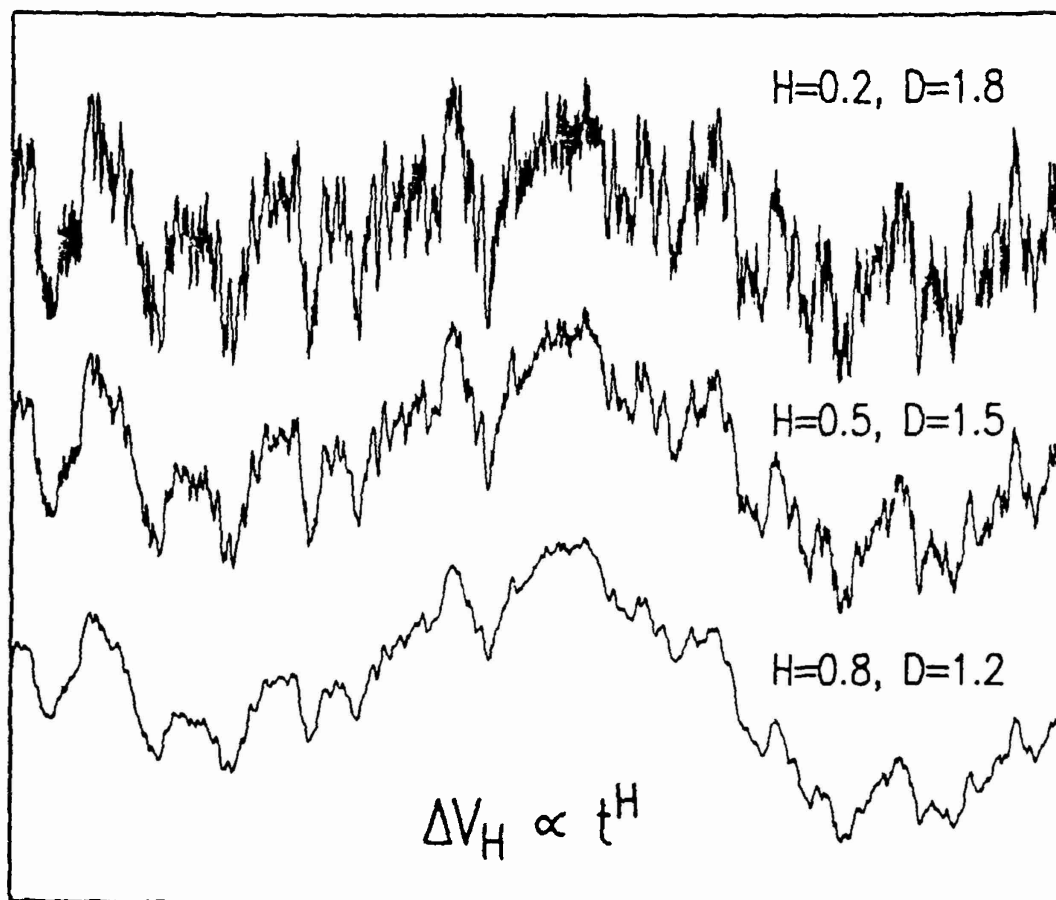


Figure 6



t, time

Figure 7

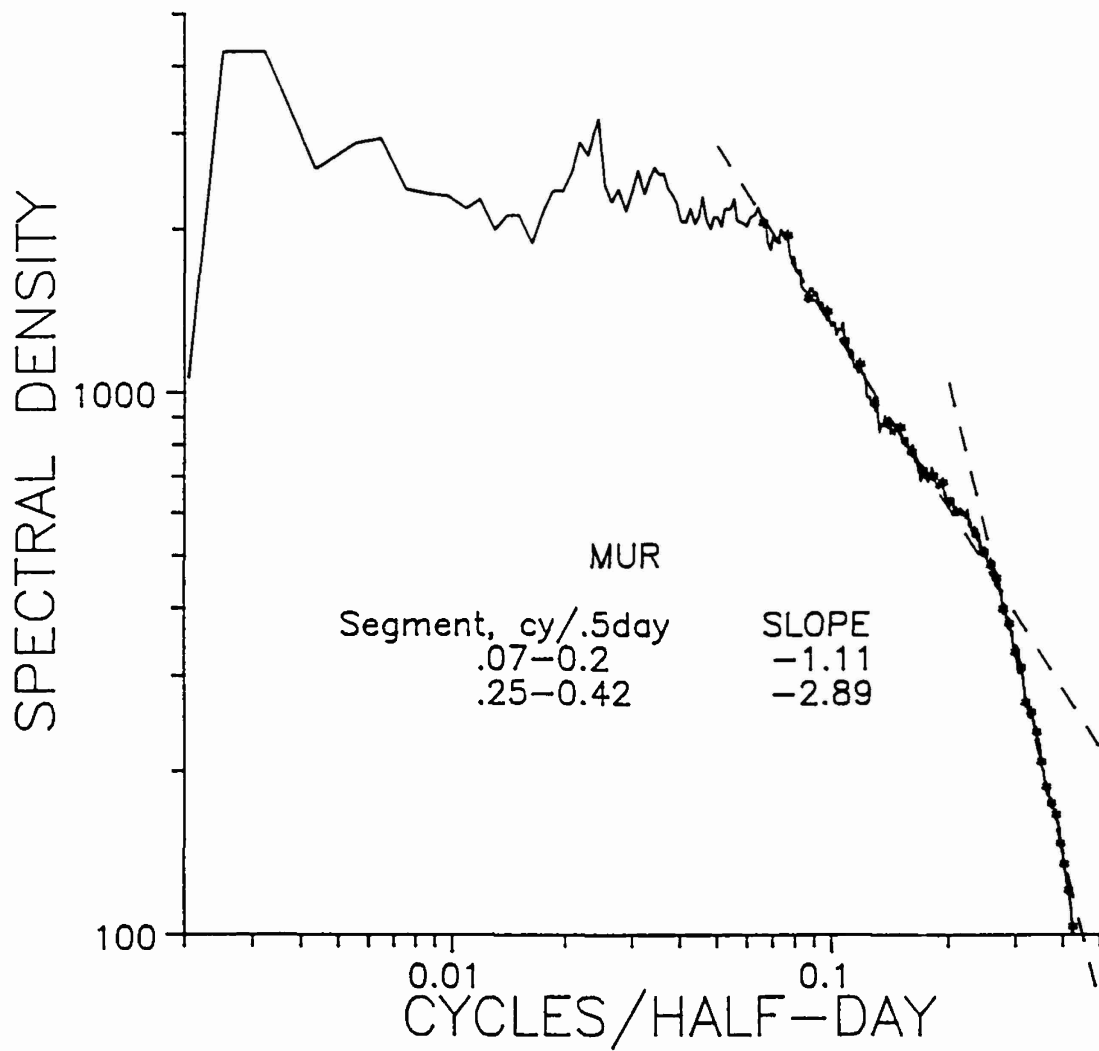


Figure 8

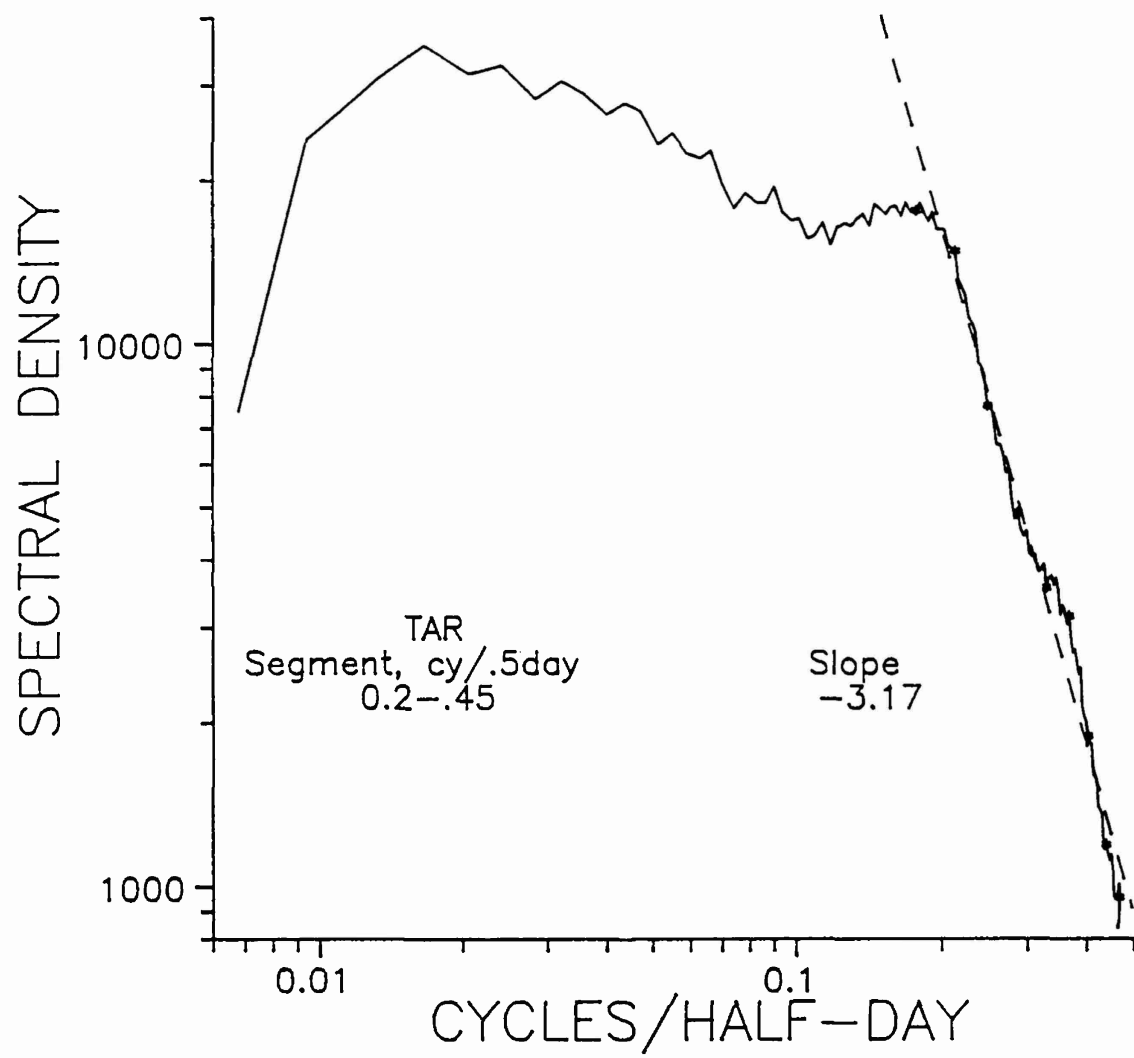
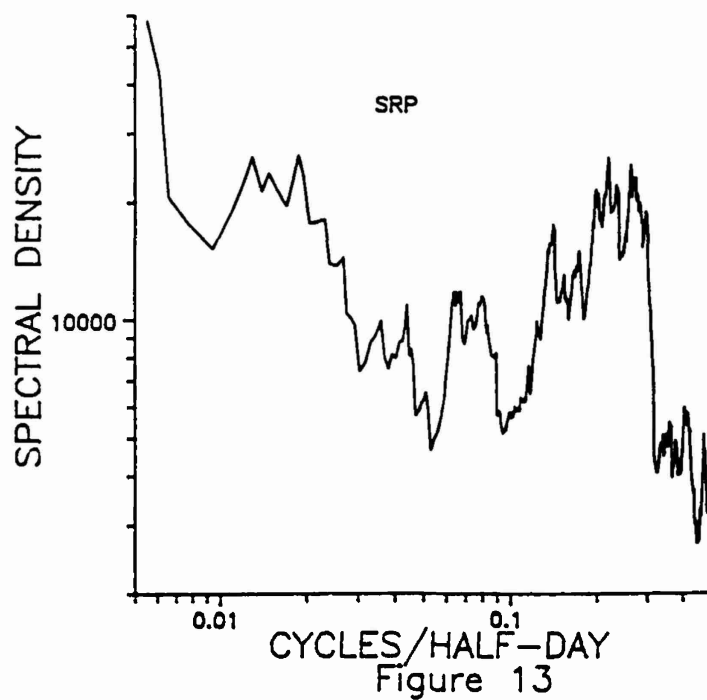
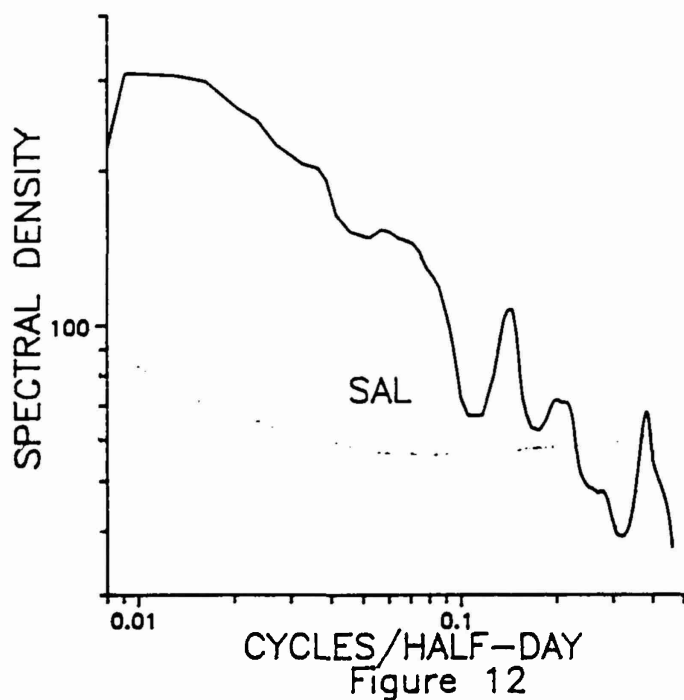
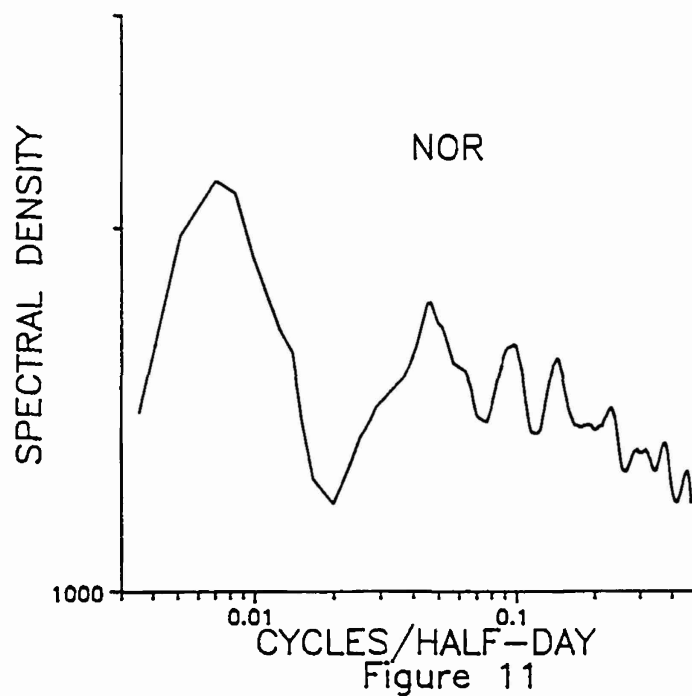
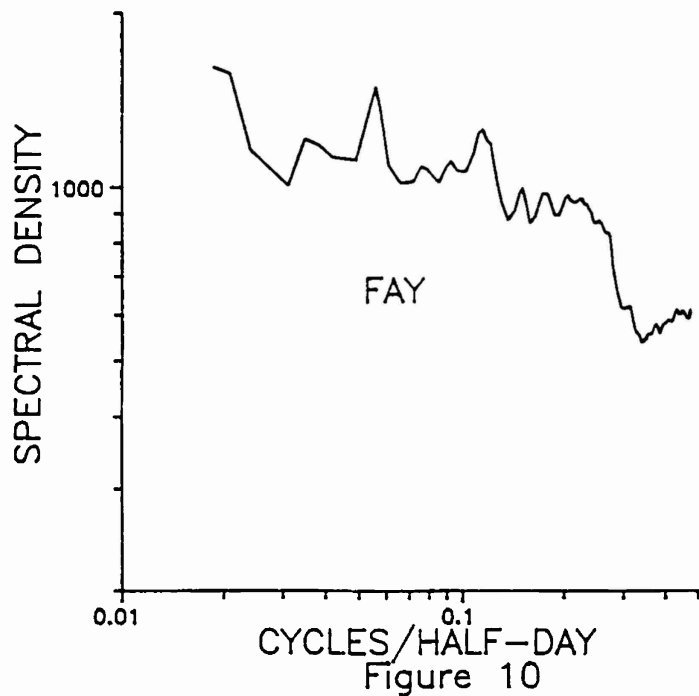


Figure 9



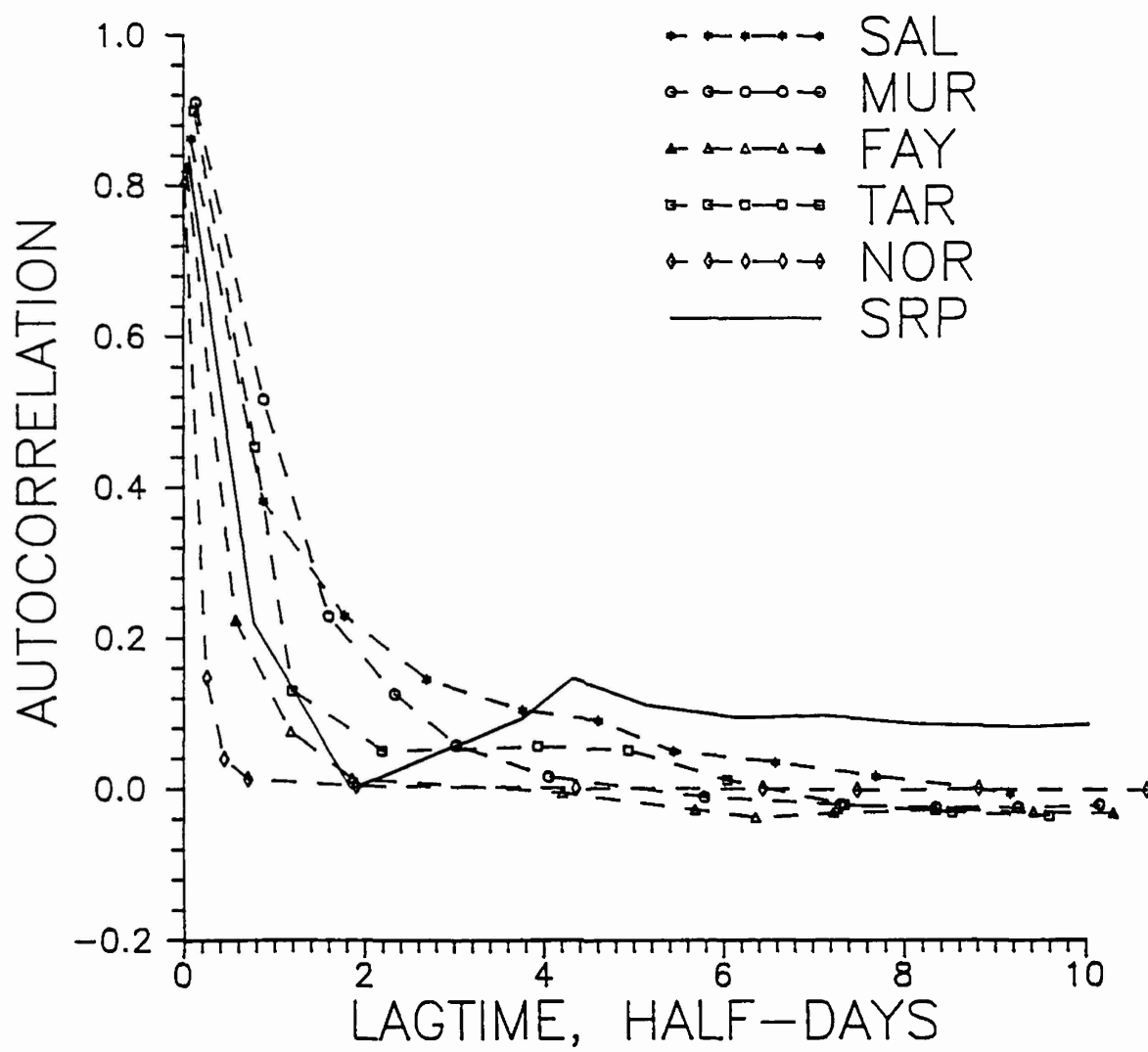


Figure 14

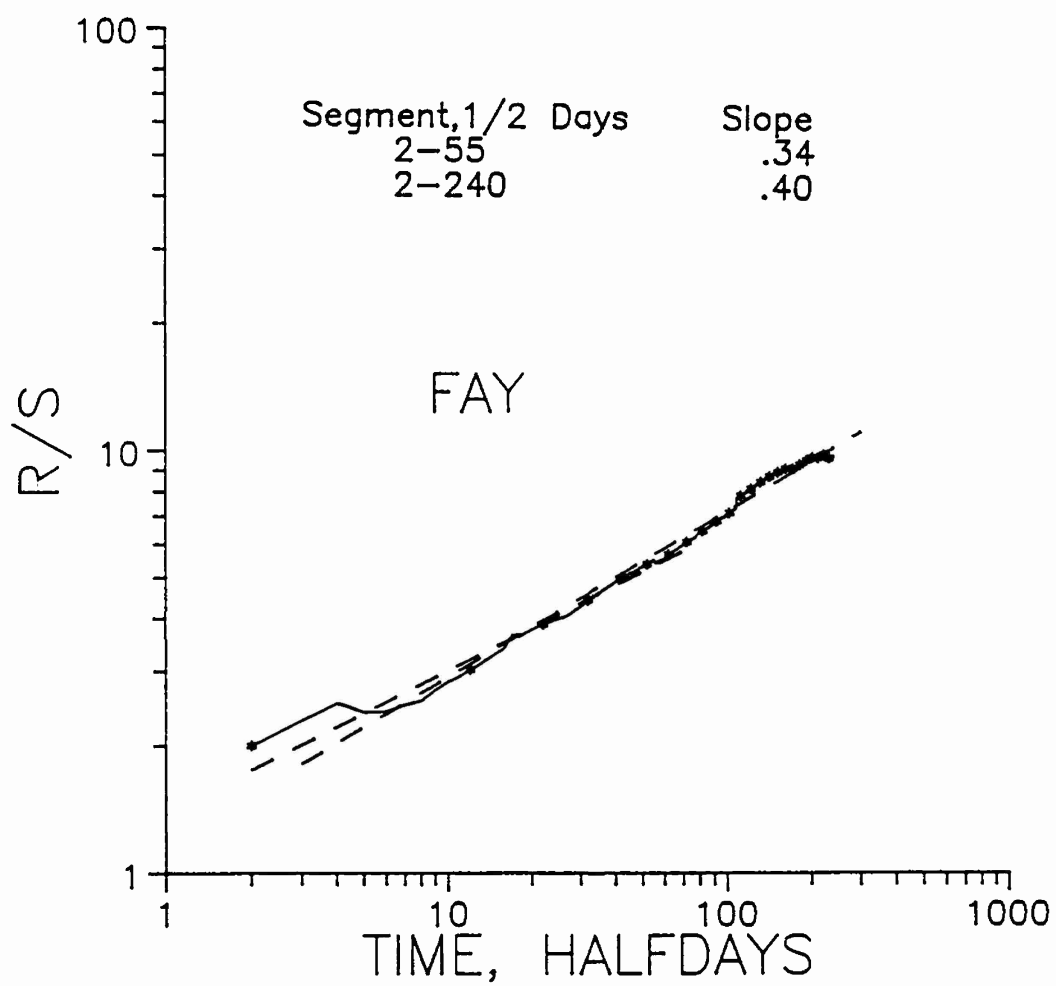


Figure 15

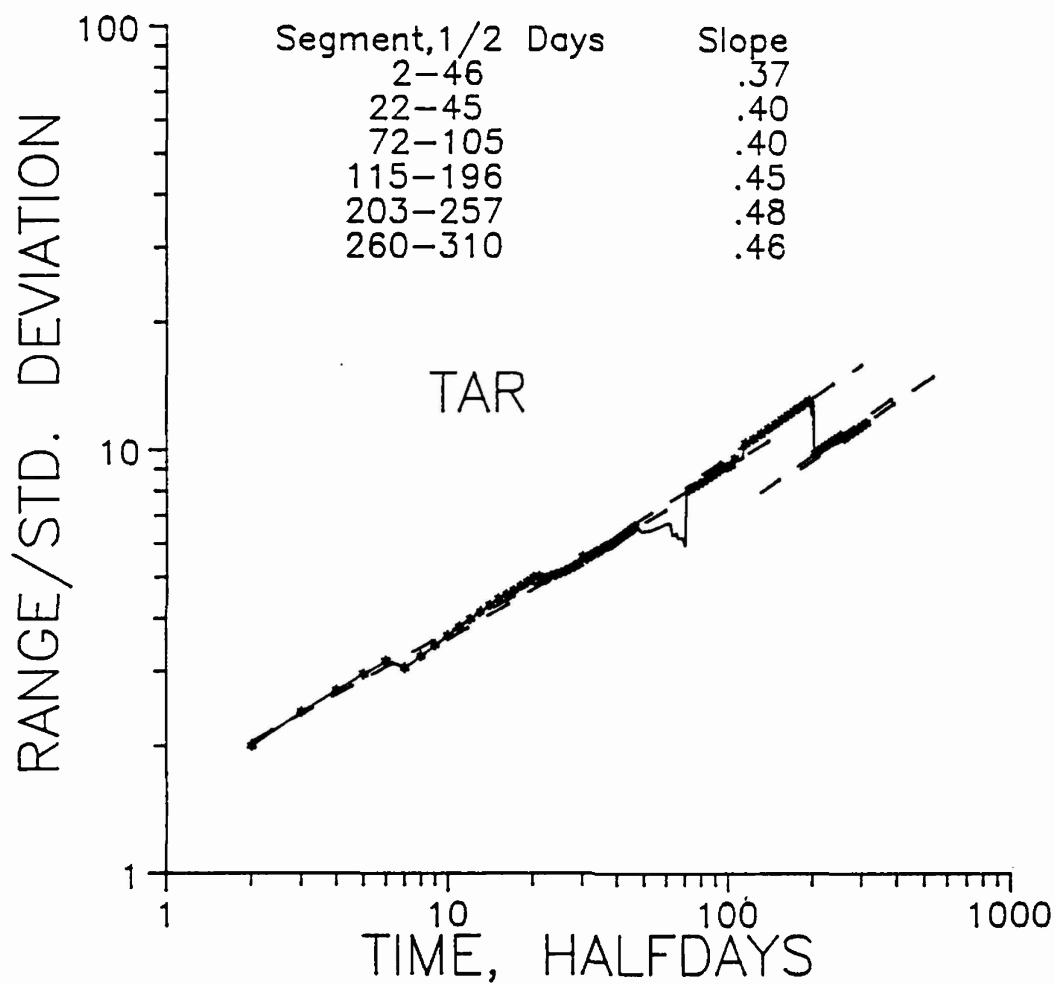


Figure 16

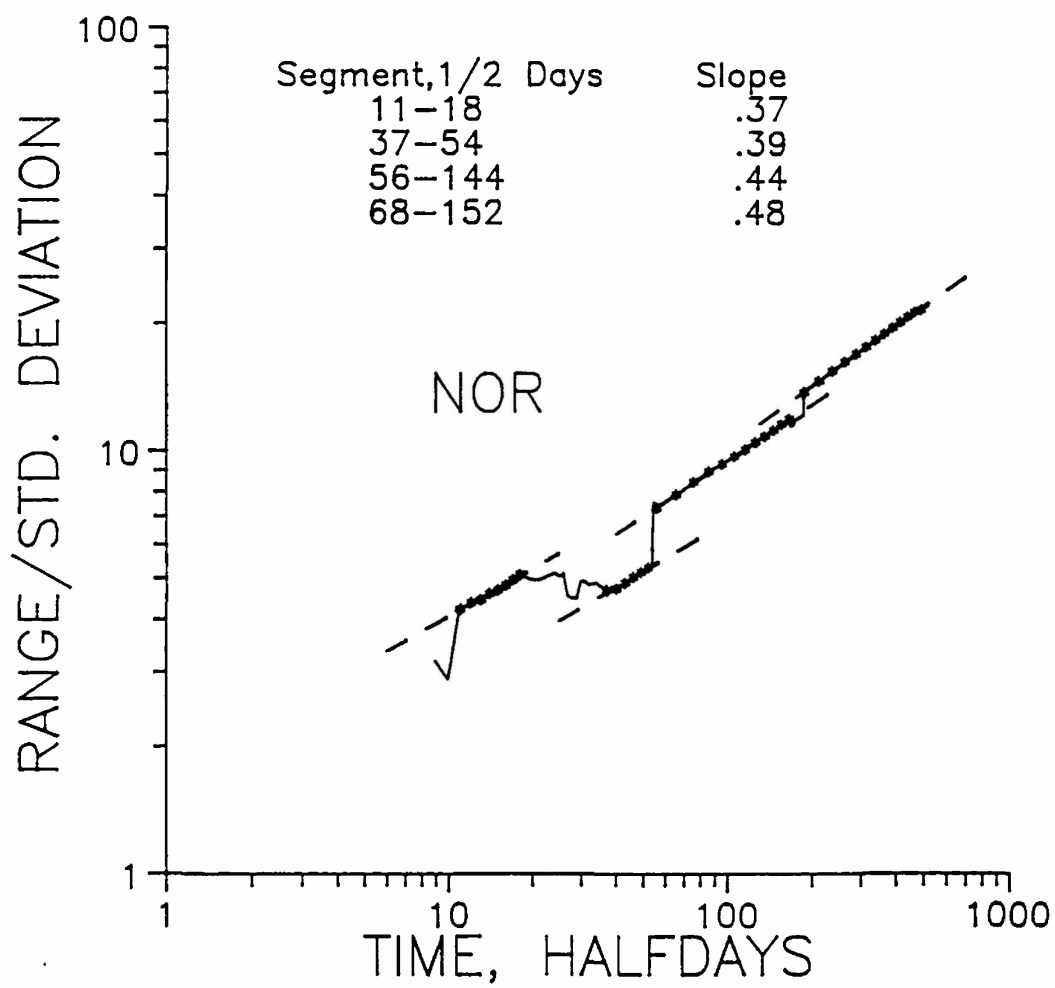


Figure 17

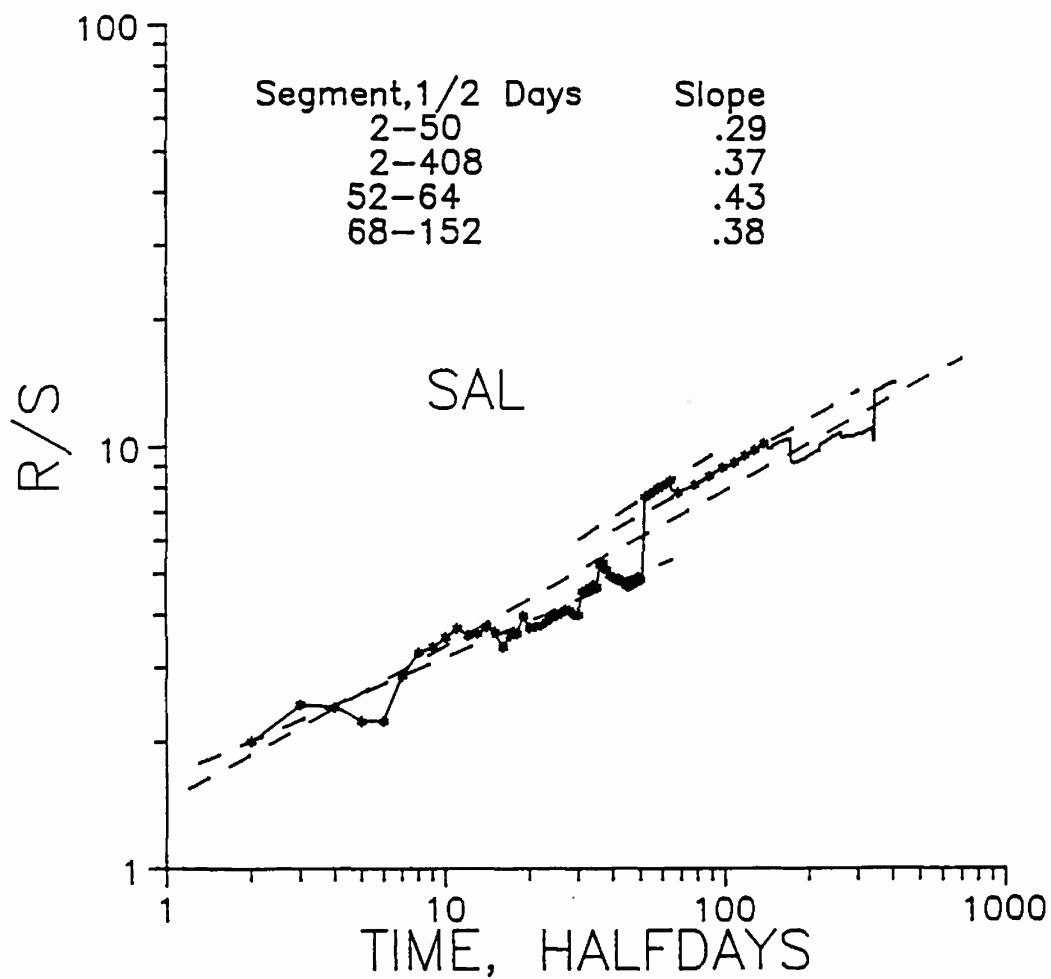


Figure 18

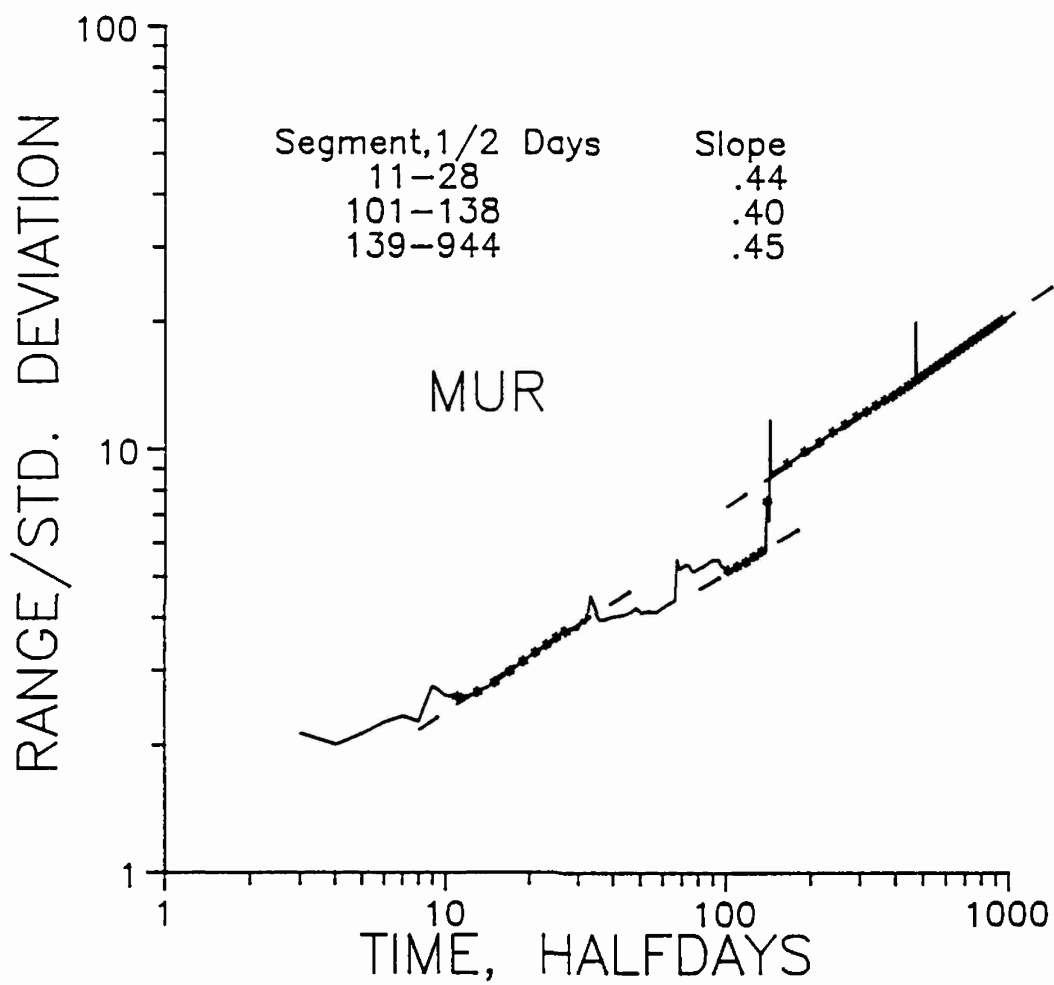


Figure 19

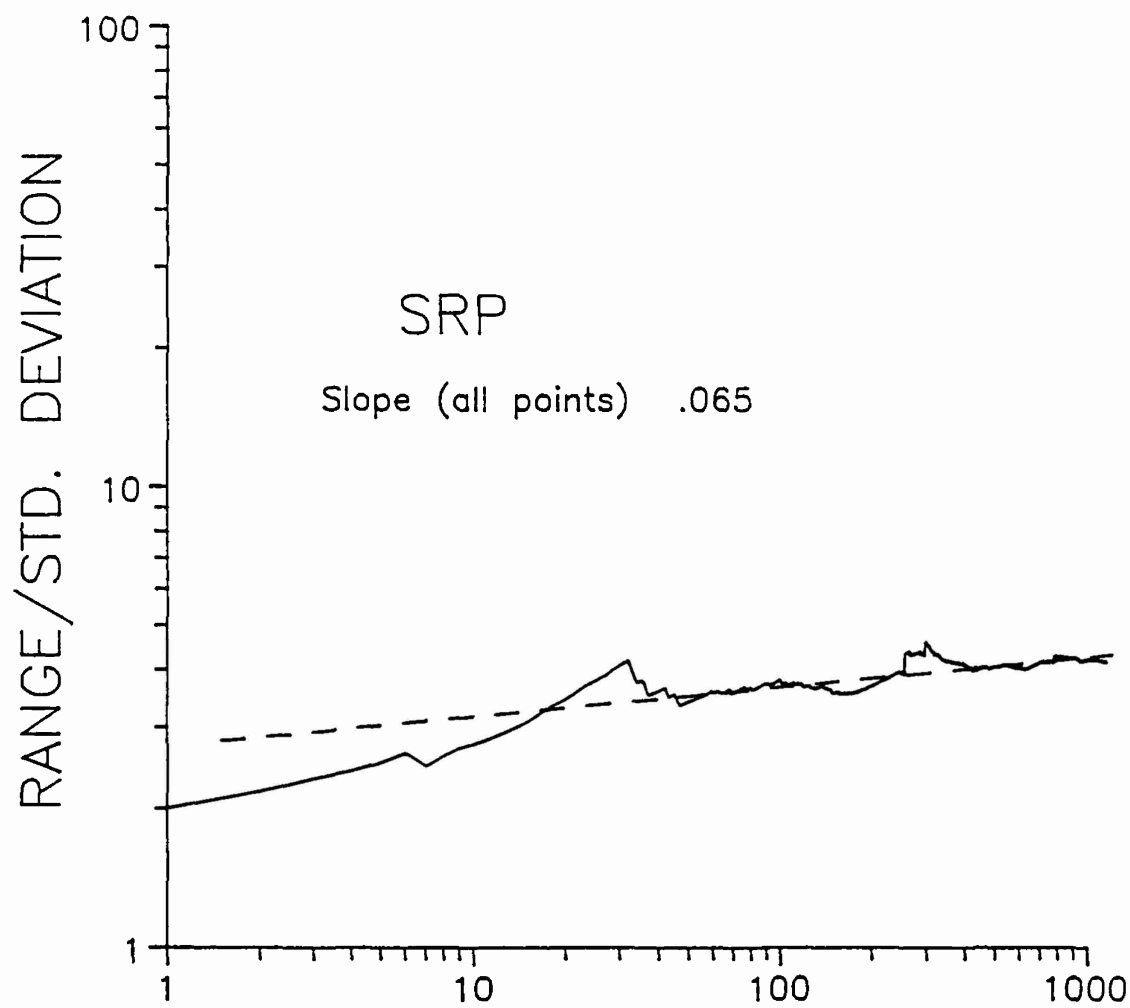


Figure 20

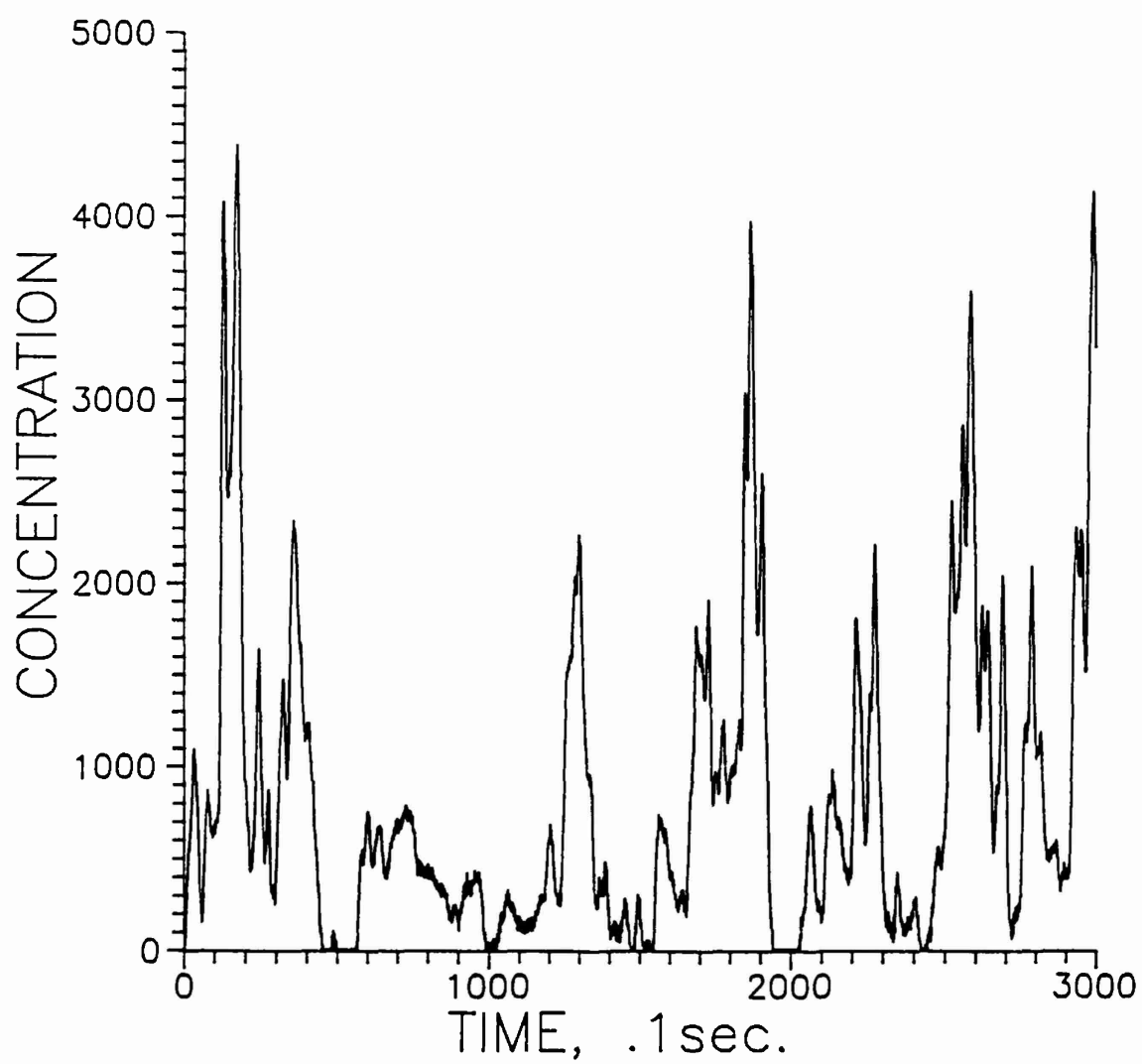


Figure 21

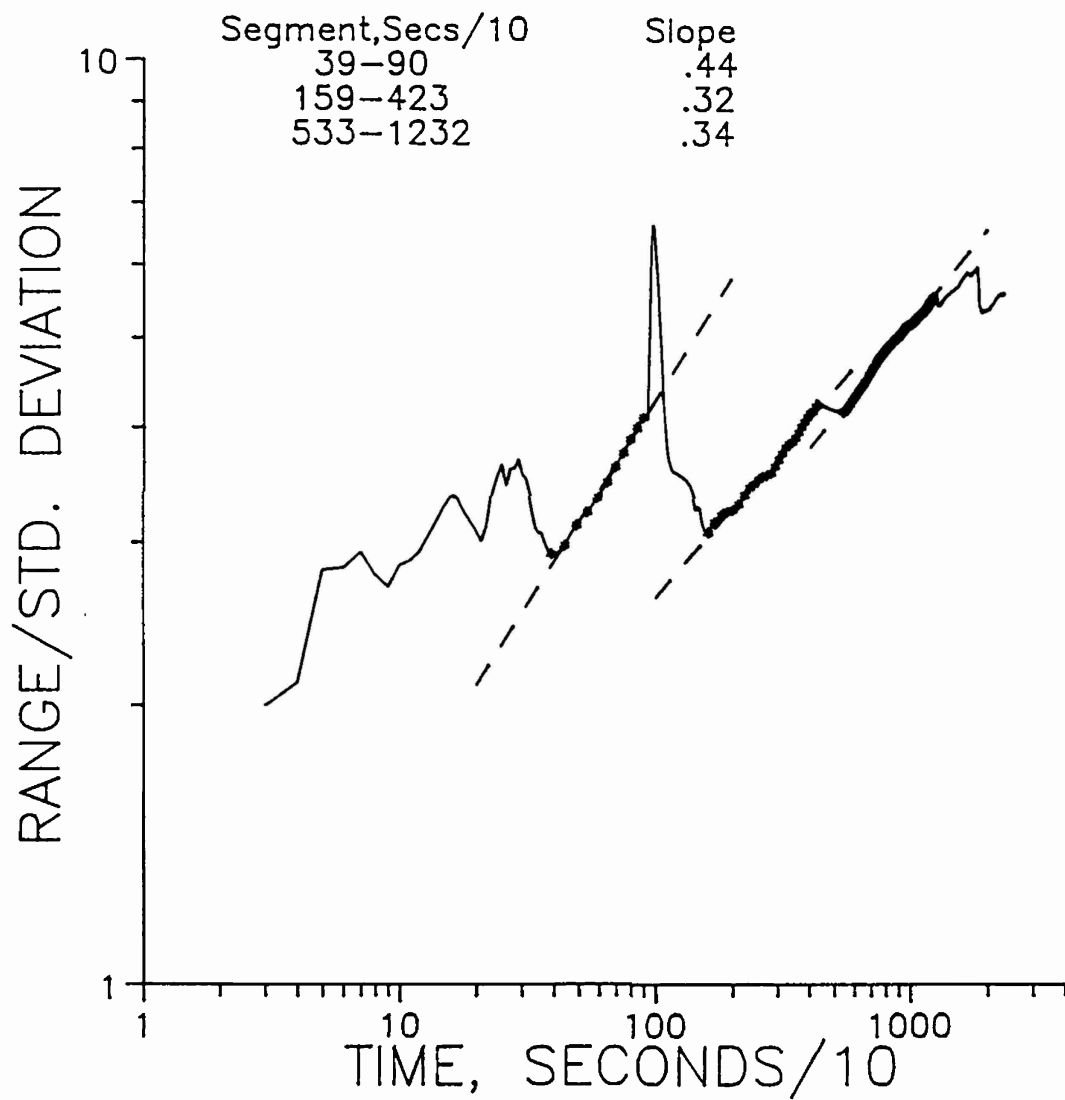


Figure 22

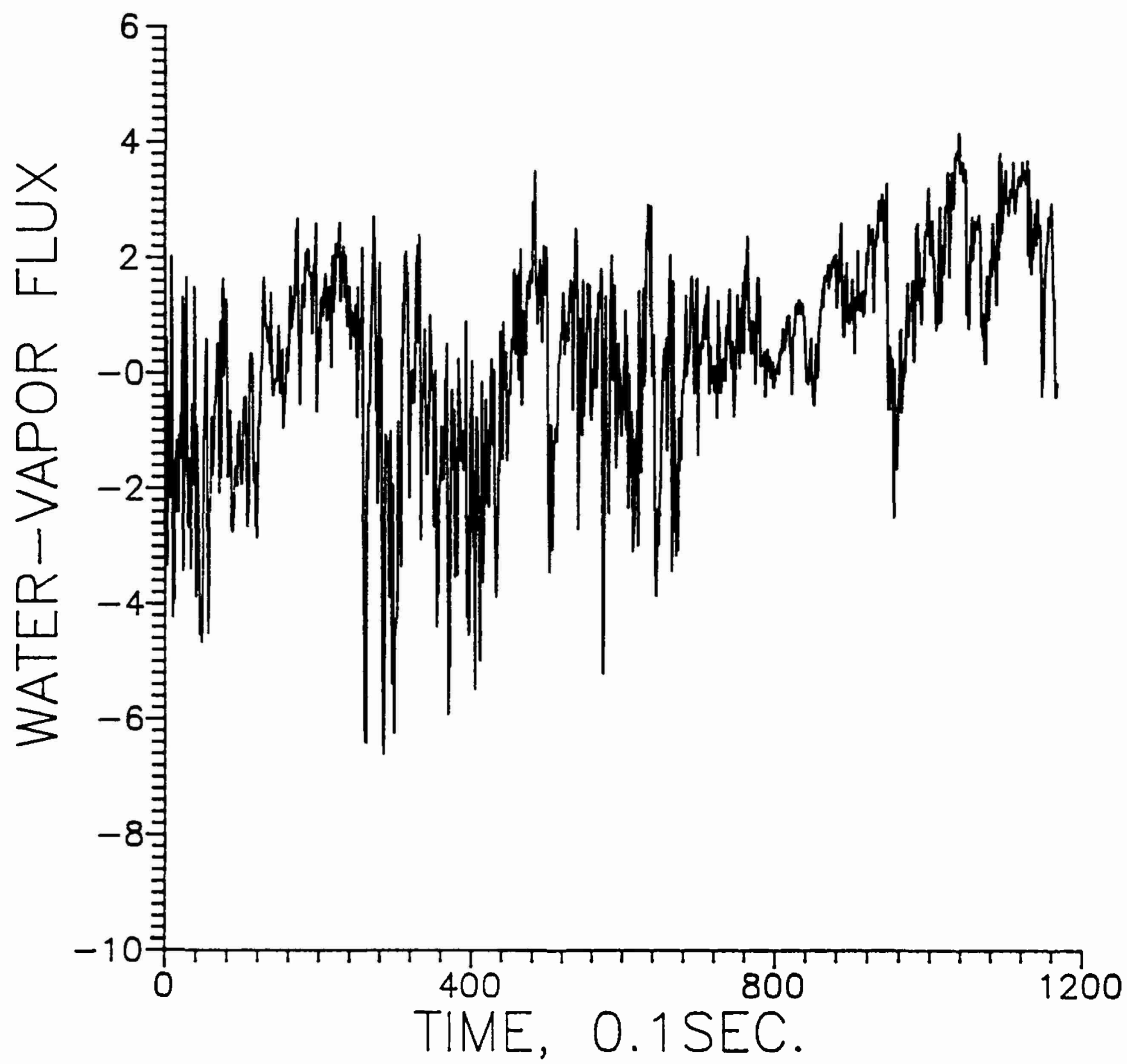


Figure 23

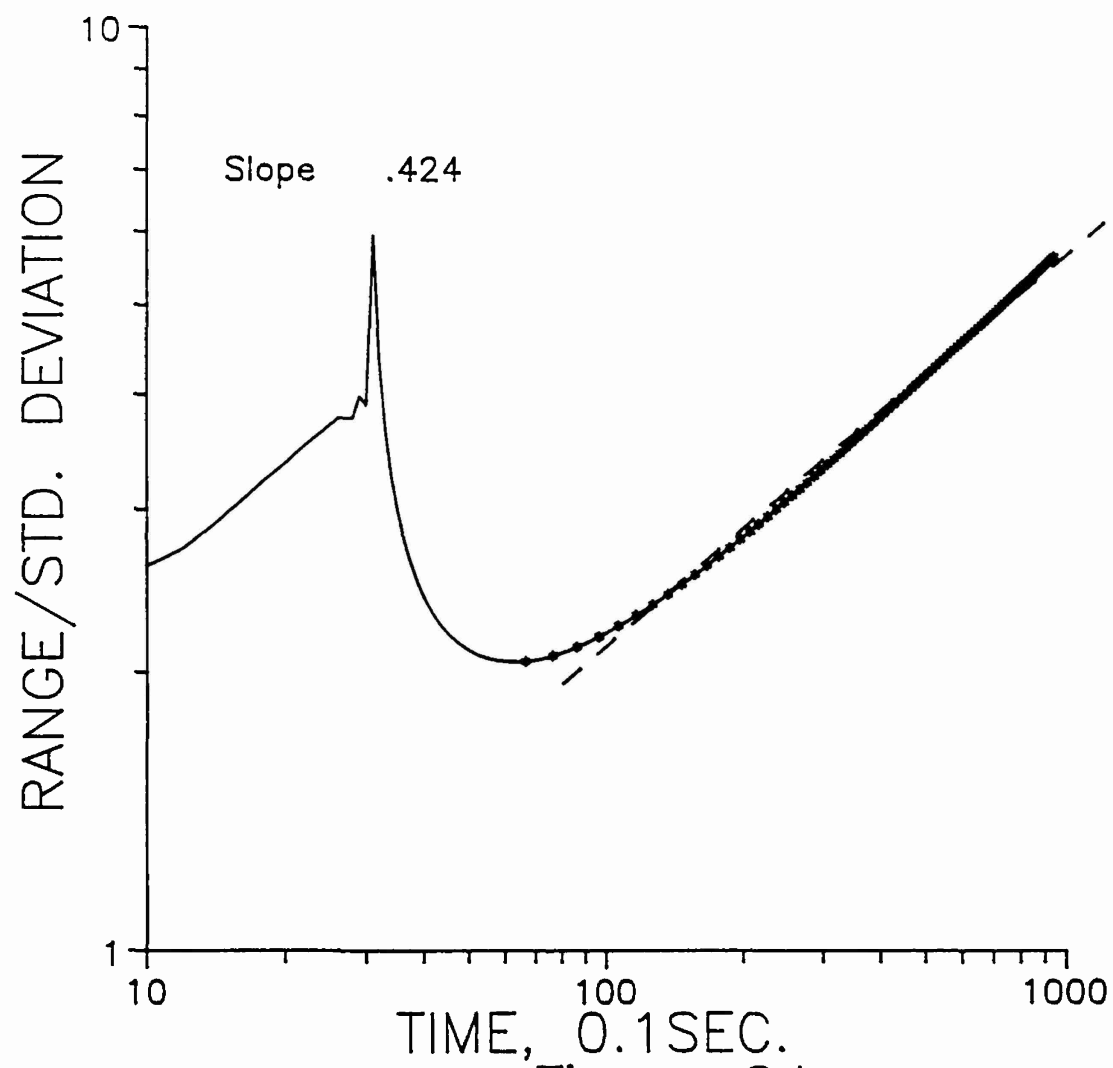


Figure 24